RHO 38

WATER TURNOVER IN HIMMERFJÄRD 1977
- a simulation study

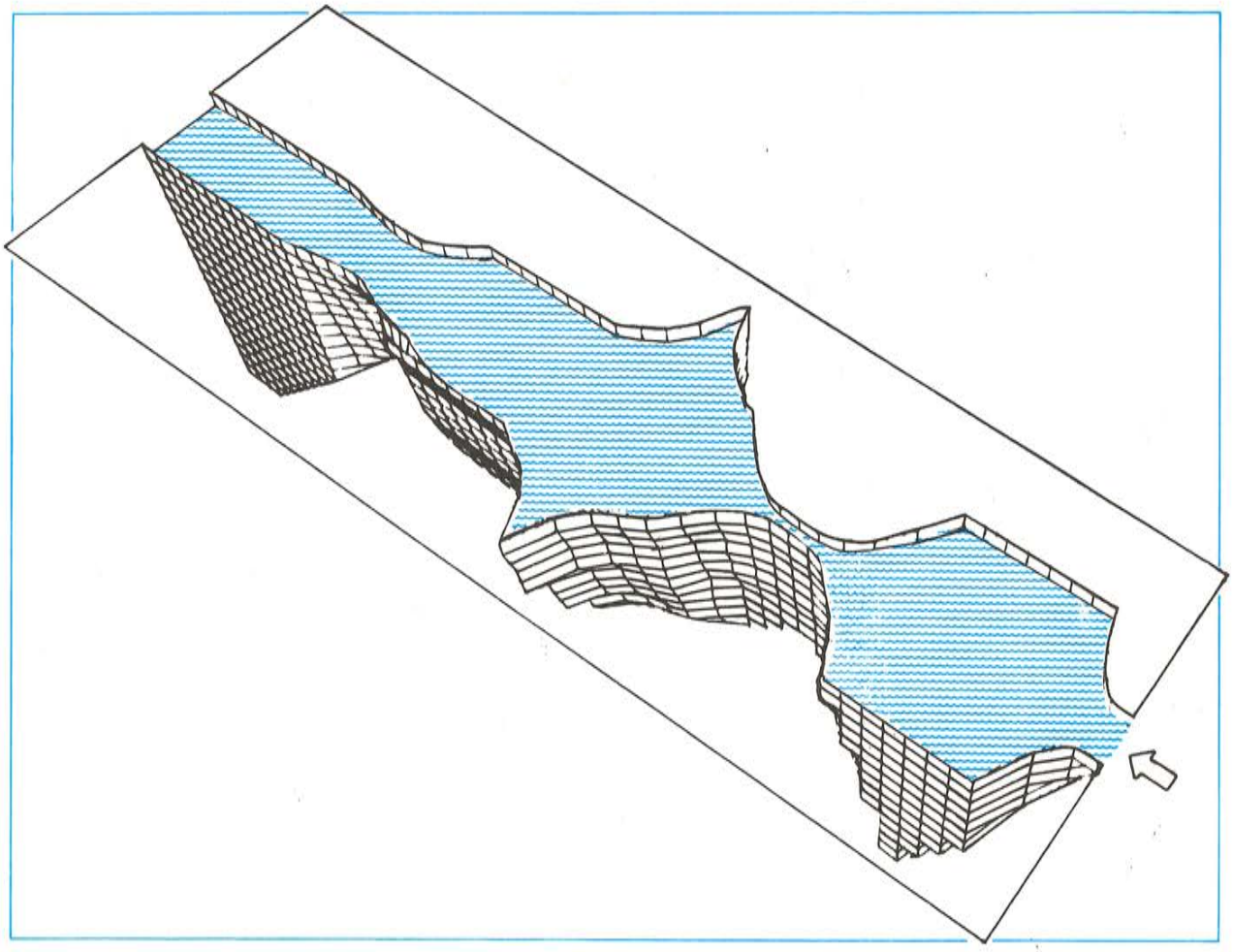

Anders Engqvist and Jonny Svensson

SMHI SWEDISH METEOROLOGICAL AND HYDROLOGICAL INSTITUTE

SMHI Reports
Hydrology and Oceanography

RHO 38

WATER TURNOVER IN HIMMERFJÄRD 1977
- a simulation study

Anders Engqvist and Jonny Svensson

SMHI:s tryckeri 1984

Issuing Agency
SMHI
S-60176 Norrköping
Sweden

Report number
RHO 38

Report date
1984-11-30

Author (s)

Anders Engqvist
Jonny Svensson

Title (and Subtitle)

WATER TURNOVER IN HIMMERFJÄRD 1977 - A SIMULATION STUDY

Abstract

A two-dimensional circulation model (one vertical, one horizontal axis) was validated for a 3-week period, taking place in early fall 1977. For this time there exists independent measurement-based estimates of the water turnover in Himmerfjärd estuary. Indata (forcing) of the model are: N/S-component of the wind velocity, freshwater flow, changes in water level and salt and temperature changes at the model border towards the Baltic. The validated model was run with the same parameter set-up for four other 3-week periods, distributed over the year 1977 to cover the different main circulation modes. Disregarding the simulation of winter situation with ice, the results seem reasonable. By the aid of a hypermodel the results of these runs were interpolated to encompass a first coarse but approximately correct whole-year estimate of the water transport in the sounds adjacent to Himmerfjärd's inner basin during 1977.

Key words
Water turnover, estuary, circulation model

Supplementary notes

Number of pages
77

Language
English

ISSN and title
0347-7827 SMHI Reports Hydrology and Oceanography

Report available from:

Water turnover in Himmerfjärd 1977 - A simulation study

Page

Contents:

ABSTRACT

The growing interest in the circulation and ecology of meso-scale coastal areas has motivated us to perform this model study. Anthropogenic eutrofication of the aquatic environment leads to the need for planning tools in the forms of ecological models to establish what dominating factors determine the response of the recipient. Such models must be founded on reliable circulation and mixing computations, not only for time scales of days or weeks, but for whole seasons and years. The present study is an attempt to meet this need and to show one possible way to extrapolate complex oceanographic model results to whole-year estimates for simulations that for economical reasons are restricted to effectively cover only a minor part of the year.

A two-dimensional (one horizontal, one vertical axis) model is applied to the Himmerfjärd fjord on the Baltic coast. The driving forces in the model are wind, river flow, water level change, and density field at the model border to the Baltic. The simulation results are hourly horizontal and vertical transports of water and dissolved matter, produced by currents and mixing, for later use in ecological considerations, mainly nutrient budgeting.

A verification study is carried out by comparing simulated and measurement-based computed water transports. The validation time period takes place in early fall when wind and current fluctuations are representatively intense. The choice of this period must therefore be deemed as a critical and decisive test of the model. The result yields a reasonably good agreement among these data during the verification period. The whole-year turnover estimate is based on four seasonal case studies, each with a duration of three weeks. The following were chosen: (1) winter situation with ice; (2a) spring bloom; (2b) spring flood; (3) summer stratification; (4) fall isothermal situation. To fill the gaps between the simulation periods, a dependence between the different flows and the forcing data, known for the whole year, is deduced. The three components water level-driven flow, estuarine flow and wind-driven flow are employed. The first one is measured independently at two stations ca 20 km apart, giving almost perfectly coinciding data. The latter two are obtained by a scatter-diagram correlation technique, and the resulting relationships are summed up in the form of a simple hypermodel that is run for the entirety of the year 1977. For the whole-year estimate of water flow, there is a high degree of explanation ($r^2 \sim 0.8$) between the circulation model and its hypermodel for the various seasons when their data are given simultaneously. Disregarding the simulation of the winter period with ice, we believe that these computations represent a first coarse, but approximately correct, whole-year estimate of the transport in Himmerfjärd.

INTRODUCTION AND ACKNOWLEDGEMENT

Water turnover estimates for Himmerfjärd are badly needed for the ecological studies that have been going on for almost a decade. The desirability of circulation estimates is, however, counterbalanced by their inherent unavailability. Field measurements that are sufficiently frequent in space and time to be useful are expensive to obtain and must also be performed with regard to the heavy boat traffic through the entire estuary.

There seems in general to exist a trade-off between measuring and calculation. Less of one demands more of the other and vice versa, down to a certain amount that cannot be substituted. Since a program with emphasis on measuring has been ruled out for the reasons cited, the necessity of the complementary approach is obvious. Organized and systematic calculations are equipollent to modelling which thus forms a possible resort from the above-mentioned dilemma between desirability and inaccessability.

When we started to implement the circulation model for the Himmerfjärd estuary, we were overly optimistic about the time the project would demand but rather pessimistic about the expected utility of the results. We feared the sparsity of the input data would be fatally reflected in the realism of the output ditto. This report shows that both these attitudes were ill-founded, which in this case is to be preferred in the place of having the dubious pleasure of being right.

The successful completion of this stage has had many contributors. In Table 0 the respective gratitudes are deferred.

1. OBJECTIVES

Since 1975, one year after the inauguration of the sewage treatment plant Himmerfjärdsverket, the recipient areas have been under surveillance with regard to water quality as well as including water turnover studies. A gentle start in 1976 when the first current measurement was performed (Bergstrand, 1977) was followed by a number of different approaches both on the theoretical and field experimental side. The accumulated work towards assessment of the water turnover has been reviewed by Bergstrand (1980) and Engqvist (1982). A major conclusion by the latter author was that because the field program of 1977 was mainly designed to provide a numerical circulation model with data, the possibility of employing simple box models based on salt balances for water turnover purposes must fail.

Short of funding for a renewed field-data sampling program, the only remaining recourse was thus to implement the above-mentioned tacitly intended circulation model for the Himmerfjärd estuary. This work was begun in summer 1982 as a cooperative project between A. Engqvist, ZISU and J. Svensson, SMHI. A primary goal was to run the circulation model for a three-week period, corresponding to the beginning of September 1977 for which time field data-based estimates computed by Toll (1980) existed. A secondary goal was later formulated in accordance with the needs of involved ecologists: To extend the simulations to cover a whole biological year. Initially the model was run on the UNIVAC 6400 computer at SMHI, but was later transferred to CD170 at QZ, Stockholm, for practical and economical reasons. In spite of the lower computer costs thus achieved, the low budget level of this project necessitated the secondary goal to cover a series of characteristic circulation modes distributed over the biological year. It was hoped that a rough estimate of yearly water turnover could be derived from such a piece-wise approach.

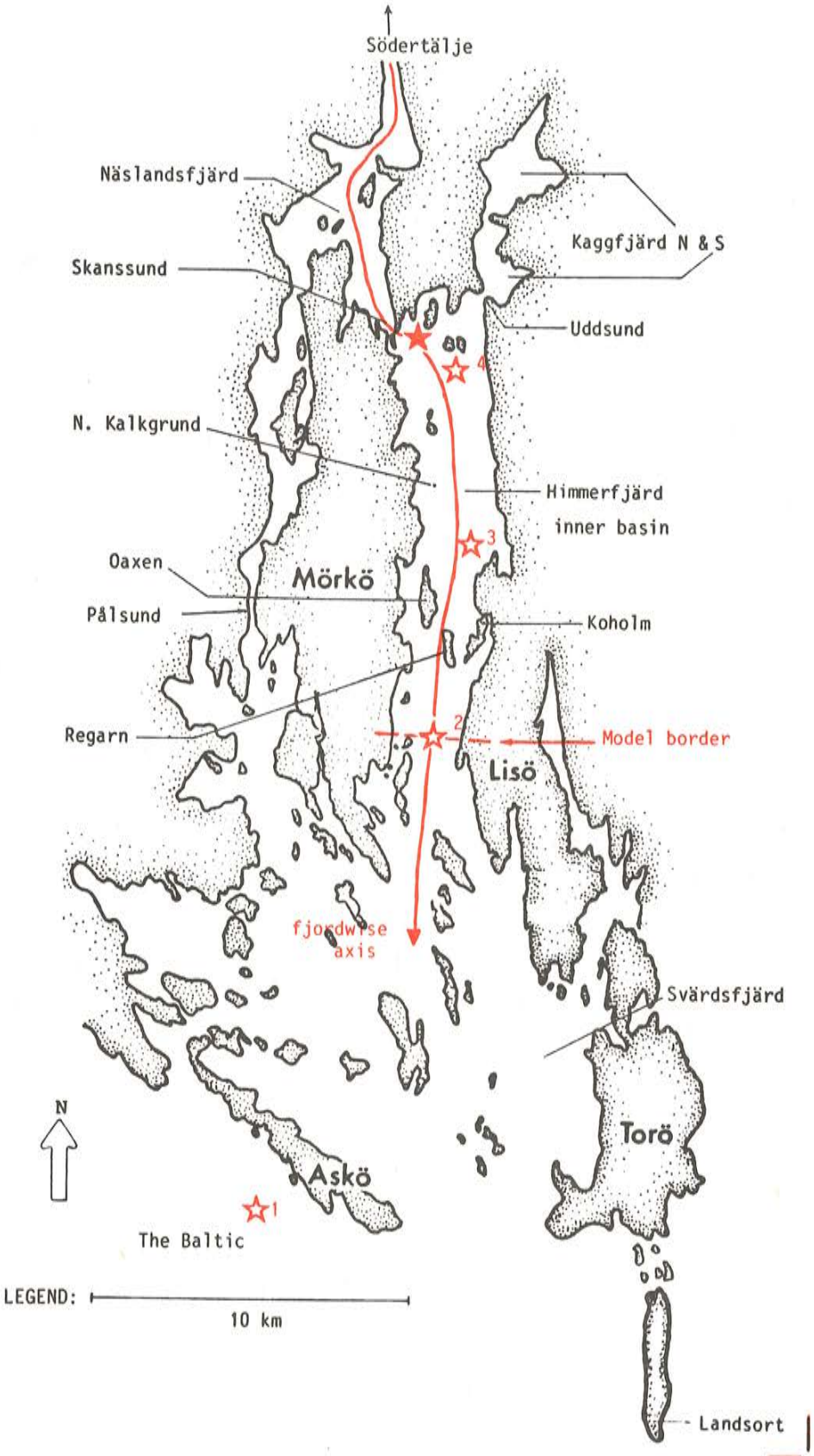

Figure 1. Overview of Himmerfjärd and its adjacent sounds. . The solid star denotes the place where the cleaning plant outlet discharges into the Himmerfjärd water. The non-filled stars indicate the respective sample sites. Star #2 two of these coincide with the model border towards the Baltic. The inner basin has the approximate position: N59°, E17°.

2. CIRCULATION MODEL

The Himmerfjärd estuary is characterized by an inner basin (see Figure 1), bordering in the northwest to Näslandsfjärd at Skanssund, northeast to Kaggfjärd at Uddsund and in the south to waters in an intermediary zone to Svärdsfjärd, and ultimately to the Baltic via the three sounds defined by the islands Mörkö, Oaxen, Regarn and Koholmen (ORK), respectively. A small passage on Mörkö's western side shunts the waterflow through Himmerfjärd over Pålsund. The major estuarine flow is dominated by the freshwater tap from Lake Mälar, and thus a natural way to define an axis alongside the fjord is through Skanssund (SS) and the southern sounds. Since the width of the fjord perpendicular to this fjord-wise axis is much less than the length scale along it, a suitable description for this study could be based on a canal assumption. This means that the fjord is described in a two-dimensional grid, one axis fjord-wise and the other in the vertical. All lateral variation perpendicular to this vertical grid would therefore be assumed averaged. Rattray and Hansen (1962) have formulated such a two-dimensional model where the hydrodynamic equations are chosen so as to alleviate the numerical computations. To achieve this objective, stream function and vorticity fields were chosen to define the advective and diffusive exchange respectively between gridboxes. The temperature and salinity fields form together with the state equation a basis for the gravitational forcing.

Such a circulation model has been programmed and employed in a hypothetical thermal pollution study concerning Bråviken (Wilmot 1976). Later the same model was used by Bork (1978), Svensson and Wilmot (1978) and Svensson (1980) with small modifications. The factors that (apart from its availability and the above-mentioned appropriate canal assumption) finally recommended this model was that it was the least complicated one that would take into account all the four major types of forcing for estuarine circulation:

1) Gravitational } baroclinic
2) Local wind drag
3) Synoptic wind drag } barotropic
4) Synoptic pressure

The freshwater flow and the interaction at the down-estuarine border of the model are included under 1). Since the local and the synoptic wind forcing a priori work against each other, the former through direct drag in the wind direction, the latter through Ekman transport in the opposite direction, field measurements have determined that the former one dominates.

The windstress is computed by the formula:

$$\tau_w = c_d \cdot \rho_a \cdot W^2 \qquad (1a)$$

The synoptic pressure is taken into account by a water level gauge located at Oaxen. Finally the external seiche with an almost 4-h period (Bergstrand, 1977) is superimposed as a high-frequency barotropic sinusoidal variation on water level.

The actual differential equations (see Appendix I) are numerically solved using Crank-Nicholson integration with successive over-relaxation according to Roache (1972), gaussian elimination for the implicit vertical scheme and "leap-frog" for the second derivative calculations.

3. INDATA

The accuracy of a model - however sophisticated - is directly dependent on its indata; therefore great care has to be taken to provide it with an appropriate set. Of necessity there exists the above-mentioned trade-off between the availability (i.e. the cost to attain the data) and the influence of it on the accuracy of the output. Since the sensitivity of a model's response to given indata cannot be known beforehand other than in

exceptional cases, this means an iterative trial-and-error process that hopefully converges towards a reliable result. Here follows an account of the governing principles to provide the model with the various indata.

3.1 Topography

Inherent in the canal assumption lies the fact that islands and multiple branches of the fjord must be discarded, but their influence on the water circulation is taken into account by projection to the sides, so that the corresponding vertical transect remains hypsographically the same. The two deep rifts that follow alongside the eastern and western shores of the inner basin of Himmerfjärd will thus be relocated to the model's mid-symmetry axis. Initially the topography was depicted by a progressive projection of each of transects at 500 m distance south of Skanssund, perpendicular to the fjord axis. Even from the very first version of the model, the area north of Skanssund had to be made less oblongated than in reality for gridpoint economy reasons. The rationale for this was that the circulation in the area north of Skanssund is not of primary interest.

From this rather detailed hypsographic description, a successive smoothing was carried out, as it was found that a minute description did not enhance the realism, but on the contrary caused numerical instabilities. Eventually the Himmerfjärd inner basin was modelled as a "bathub" with homogenous transects, harmonically interfacing the adjacent sounds, of which the transect area of the southern three were summed to give one conjoined resulting sound. In Table 1 relevant hypsographical data are listed, and the ambition to make the model, concerning surface areas and volumes, as close to reality as possible is obvious. These are the most accurate data with an estimated relative error < 2 %. The estimated sound areas are less accurate, even though they are based on best available charts. The relative error is about 10 %.

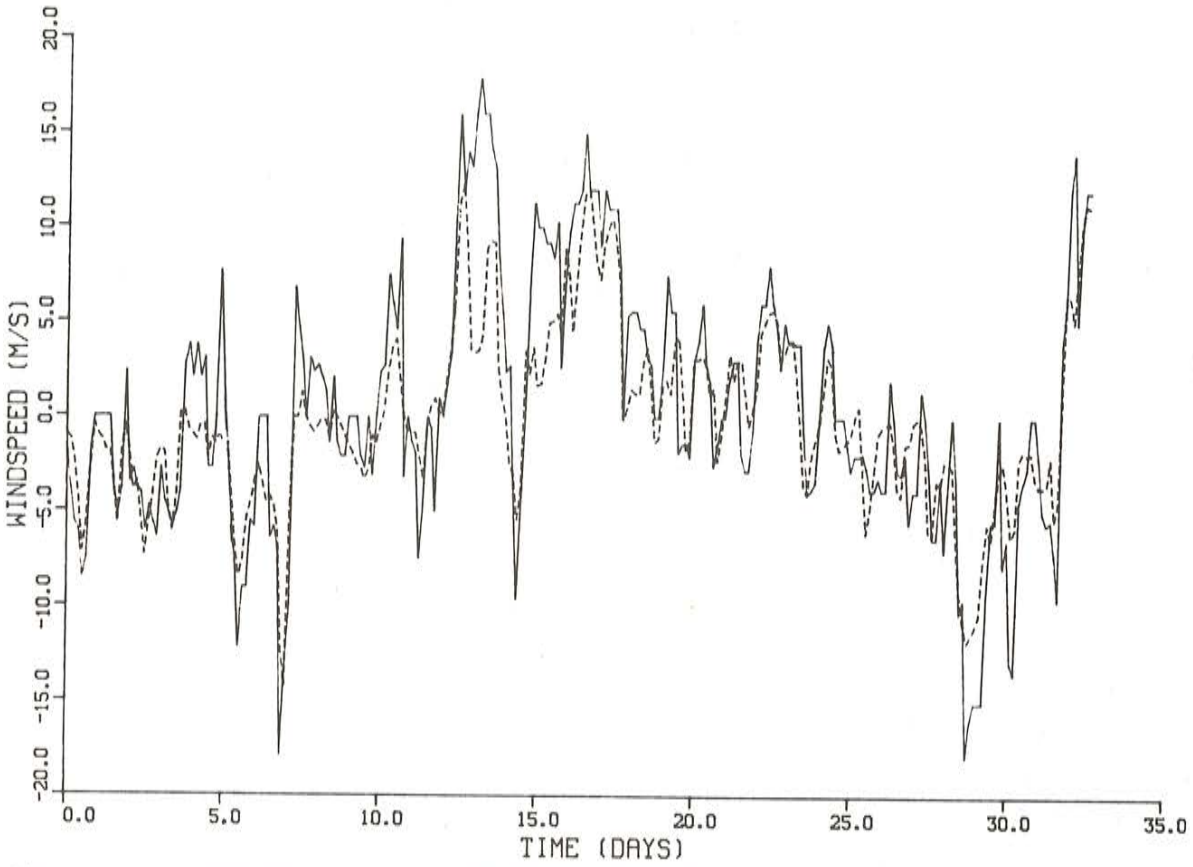

Figure 3 a. Comparison of the N/S component of windspeeds at Landsort (solid line) and at N. Kalkgrund (broken line) for 35 days, starting end of August 1977. The former is measured at a higer altitude above sea level (23m compared to 2.5m), which partly explains its sharper peaks.

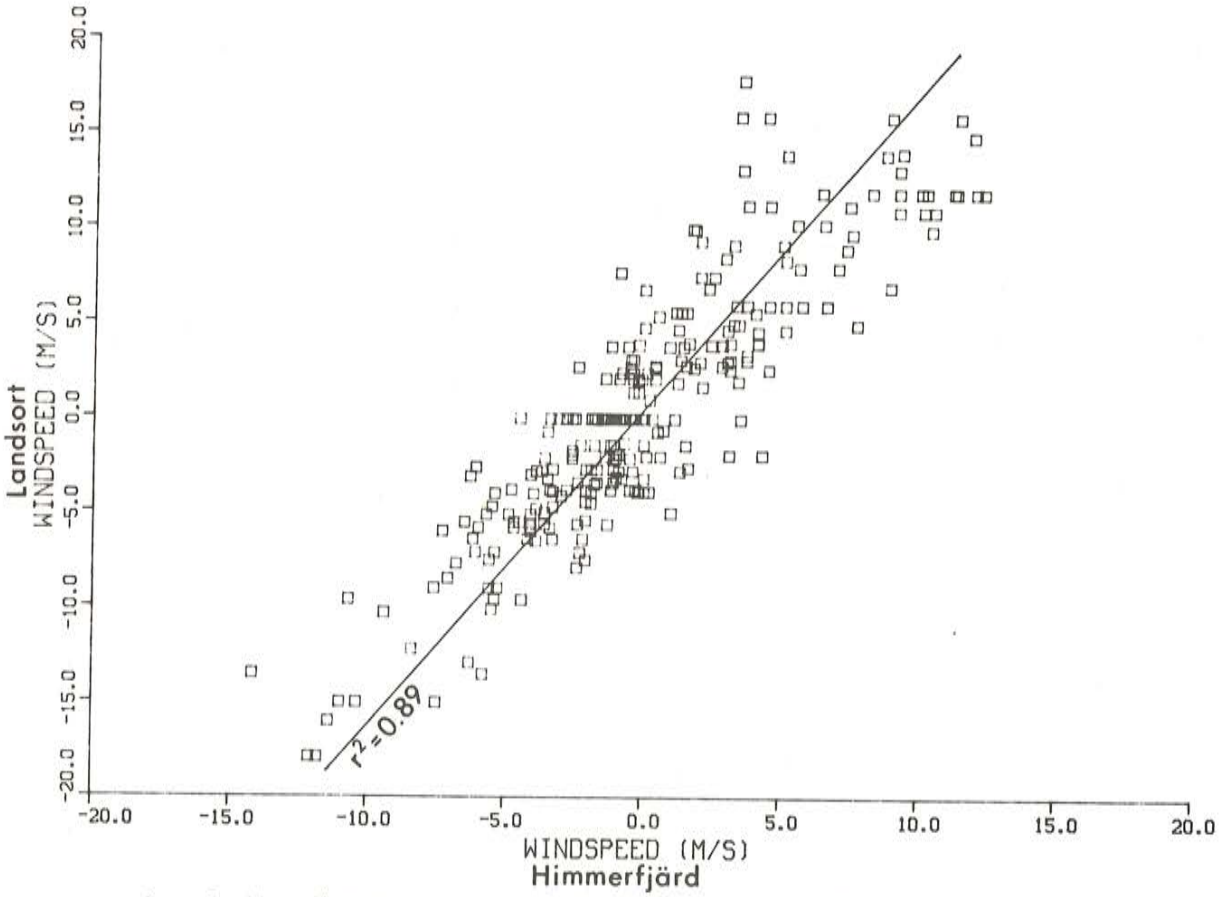

b. Scatter diagram of the two windspeeds, with the regessionline indicated. The cross-correlation factor $r^2 = 0.89$. The slope of this line is 0.62, meaning that the wind at Himmerfjärd on the average over this period is smaller by this factor than the Landsort wind.

Since the model cannot enact embranchments, the volume of Kaggfjärd had to be superimposed on the Himmerfjärd inner basin. This was necessary to ensure that the barotropic surface transports remain true for water level changes. The resulting topography is shown in Figure 2. To be sure, this gives an overestimation of the mobility of the Kaggfjärd water, and it seems to be more realistic to include only the water above the sill-depths. This consideration applies to the other adjacent fjords as well. In a first approximation a strict conservation of volumes and surfaces seems to be appropriate. The Pålsund passage has to be neglected altogether, a concession to the model approach that is deemed to be of minor importance as its transect area is small compared to the ones interfacing Himmerfjärd's inner basin.

3.2 Salt and temperature data

The salt and temperature (S&T) data used are collected by the Askö routine sampling program with a coverage of every second week, except for the ice period when there were no samples taken. During the spring bloom period a sample period of once a week was performed. From Figure 1 one sees that two stations are located in the inner basin; the third is made to coincide with the model border towards the Baltic.

To get started the model needs initial salt and temperature fields. This could of course be accomplished by an interpolating routine for making isohalines and isotherms slope in accordance to measurements. This has nevertheless turned out to be irrelevant, since the corresponding velocities cannot be provided and thus a baroclinic non-equilibrium must be discharged at any rate in the initial phase of a simulation. Instead, the following policy was adopted:

1. Fill Himmerfjärd north of ORK sounds with homogenous S&T fields that are averages of Station 3 and 4 data;
2. Fill the volume south of ORK sound with S&T fields similar to Station 2 data (border data);
3. Establish a baroclinic equilibrium after 24 h initial simulation.

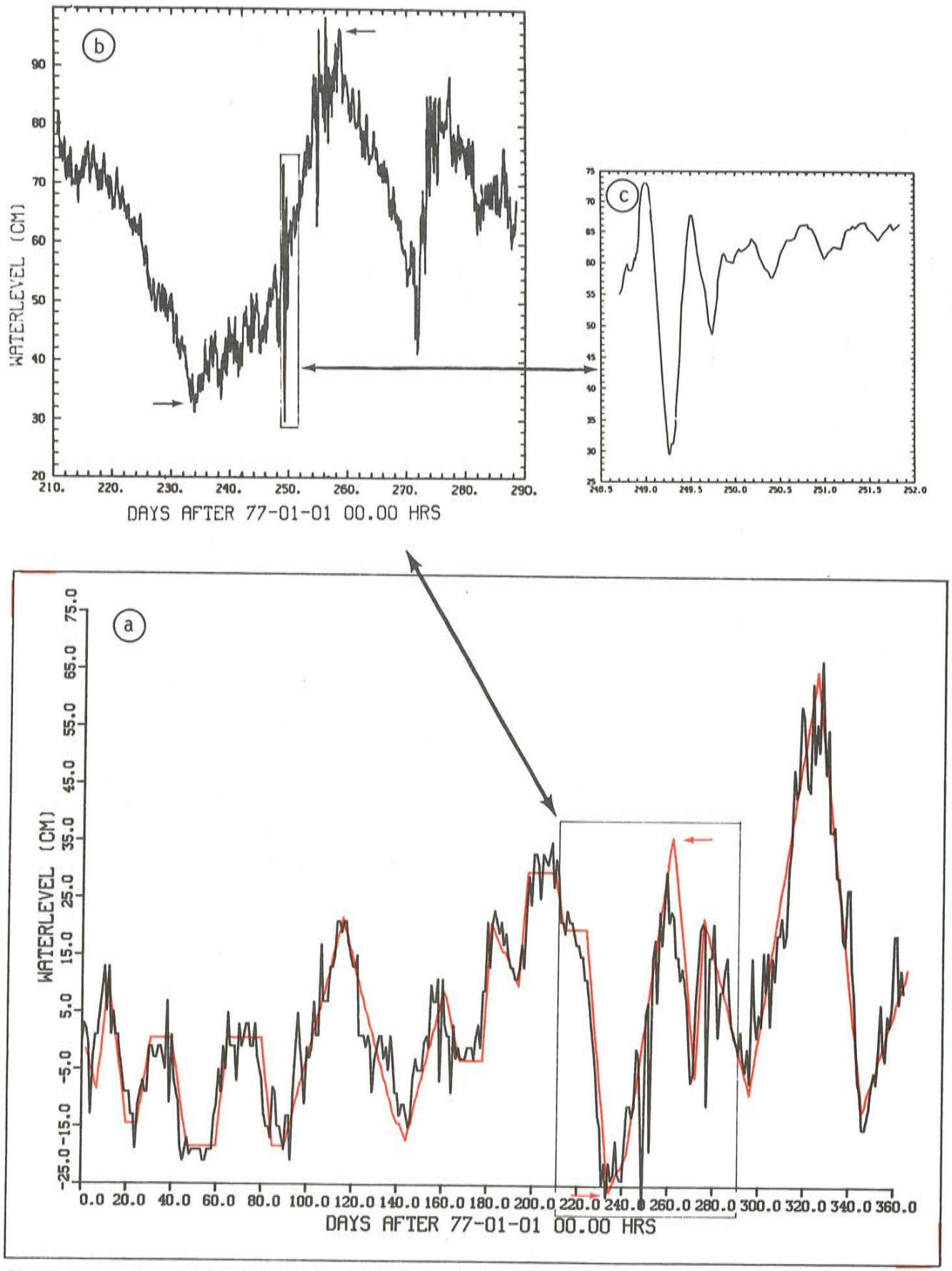

Figure 4 a. This illustrates the daily water level observations at Södertälje (black curve) and the piece-linear approximation used for simulations (red curve).

b. This shows simultaneous and independent data as Figure 4a of the water level gauge stationed at Oaxen. These data compare quite convincingly, even though the latter data is digitized more frequently, so that fluctuations due to seiches of various time periods are visible. The small arrows indicate events that are suitable for checking that the waterlevel changes in the two diagrams match over longer periods.

c. This picture is an enlargement of the most rapid water level shift that was recorded. This is accounted for in the model as caused by the windforcing.

The border data between the sample periods are assumed to remain the same, i.e. no interpolation is undertaken. For the record it must be noted that there exists more densely sampled data for the time period (Aug-Oct 1977) when the intensive measurements took place. These data sampled by SMHI are, however, not compatible with the Askö data since the two sampling programs were not intercalibrated (Engqvist, 1982).

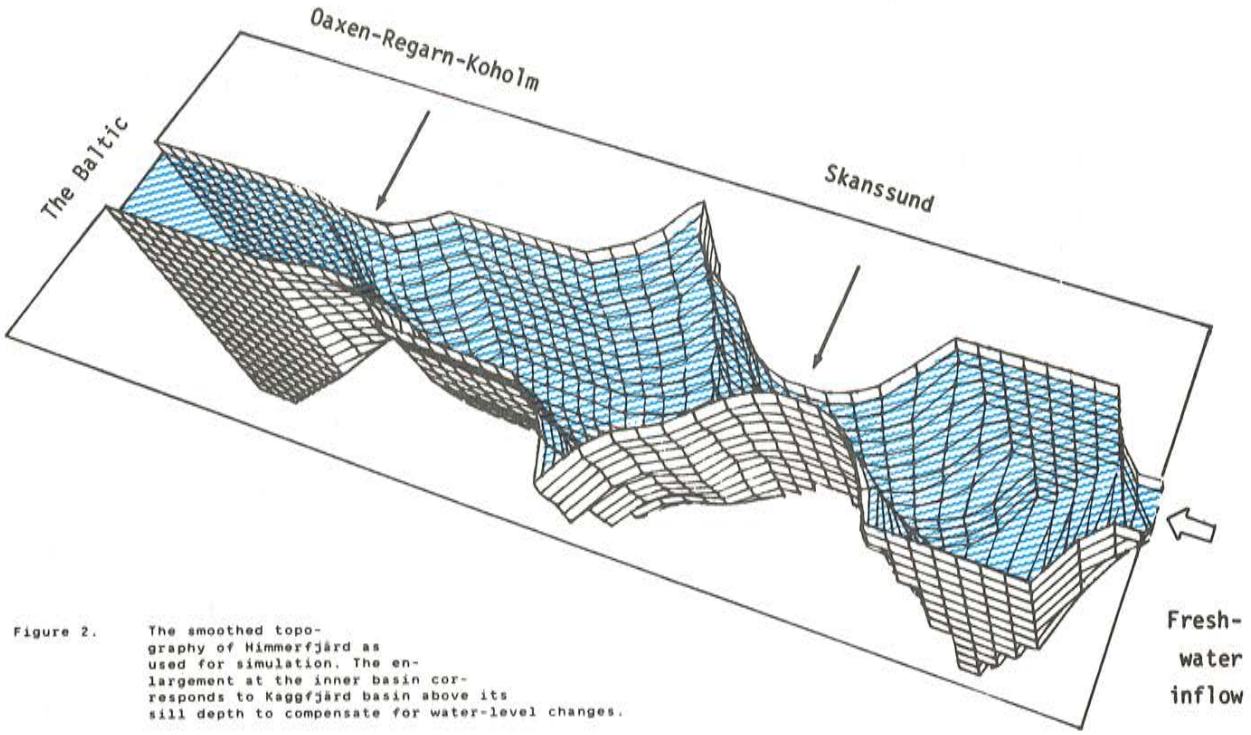

Figure 2. The smoothed topography of Himmerfjärd as used for simulation. The enlargement at the inner basin corresponds to Kaggfjärd basin above its sill depth to compensate for water-level changes.

3.3 Wind data

During most of the year 1977 local wind measurements were performed at N. Kalkgrund (see Figure 1). Because of the N/S orientation of the fjord axis and correlation studies by Engqvist (1982), only the N/S component of the wind velocity is considered in the following. A comparison for a period beginning 1 September 1977 yields that these data are quite similar to wind logged at Landsort (30 km away) by SMHI, even though the peaks are somewhat larger in amplitude (see Figure 3a). A regression line yields the wind in Himmerfjärd as 0.6 x wind at Landsort. The latter data were sampled at a 3-h interval and are to be preferred, since they are available constantly as a part of routine weather data recording. A cross-correlation (Figure 3b) for the same time period gives

r^2 = 0.89; the difference can partly be explained by the difference in measurement altitude 2.5 and 13 m above water level, respectively. For this reason the Landsort wind was chosen for wind input data.

3.4 Water level changes and seiches

The water level in Himmerfjärd was recorded in 1977 by use of a pegel gauge at Oaxen. The low-frequency component gives rise to a barotropic surface transport flow changing all water levels at the same rate simultaneously and has been fed into the model as a piece-linear approximation. In Figure 4a this piece-wise approximation is shown together with the routine water level observations at Södertälje performed diurnally by the pilots stationed at the lock there.

A comparison to the water level at Oaxen (Figure 4b) for the intensive measurement period yields an almost perfect fit with the Södertälje data, although the former is digitized more frequently. The two curves coincide for other parts of 1977 when the gauge was in order (day 0-345), but these data are not digitized. In addition to this low-frequency component, the water level record shows higher frequency seiches in the form of a superimposed ripple. The above-mentioned 4-h period can be indentified, as can smaller unimodal seiches in the Himmerfjärd inner basin with a period time T_s = 50 min given by

$$T_s = 4L/\sqrt{gD} \qquad (2)$$

where g = 9.81 m/s^2, L and D are the length and depth scales respectively. Seiches with 6-h and 8-h periods can also be detected, but are less evident. According to Toll (1980), the 4-h seiche is in phase at Skanssund and Oaxen-Regarn, which gives a rationale for taking the 4-h seiche into the model as a superimposed sinusoidal barotropic variation with an intensity of 100 m^3/s at the ORK sounds on top of the low-frequency water level changes.

In Figure 5 an overview of the data flow in the model is outlined together with its interconnection to a future distribution model. Such a distribution model has been constructed out of the simulation model and trial runs have been attempted. Its purpose is to make it possible to study the transport of any material dissolved in water (e.g. nutrient), given the advective and diffusive fields with a sufficient temporal resolution. The distribution model differs thus from the simulation model only in that these fields are not computed, but fed into it as input data.

4. PARAMETER ASSESSMENT

A model's foundation to reality - its realism - is largely reflected in its parametrization. The more physical the parameter set-up can be made, i.e. the more it can be related to other experiments, the more conclusive the model can be made. The ideal parameters can be found in experimental physics, e.g. the gravity constant which remains $6.670 \cdot 10^{-11}$ Nm^2/kg^2 universally. In Table 2 the model parameters are listed in an overview among various sources. The most controversial parameters are the first four that refer to eddy properties. The model cannot pretend to give a higher spatial resolution concerning the dynamic properties than the corresponding scales permit. Nor will the model give any better degree of realism in the simulation of the baroclinic vorticity field dynamics than is consistent with their stability over time. This will be thoroughly discussed in respective chapters following.

The molecular diffusion and viscosity parameters, although they are ultimately responsible for the local mixing and momentum transfer in nature, have only a minor influence in the model. They are thus less controversial to the same degree as they are negligible in comparison to the corresponding eddy parameters.

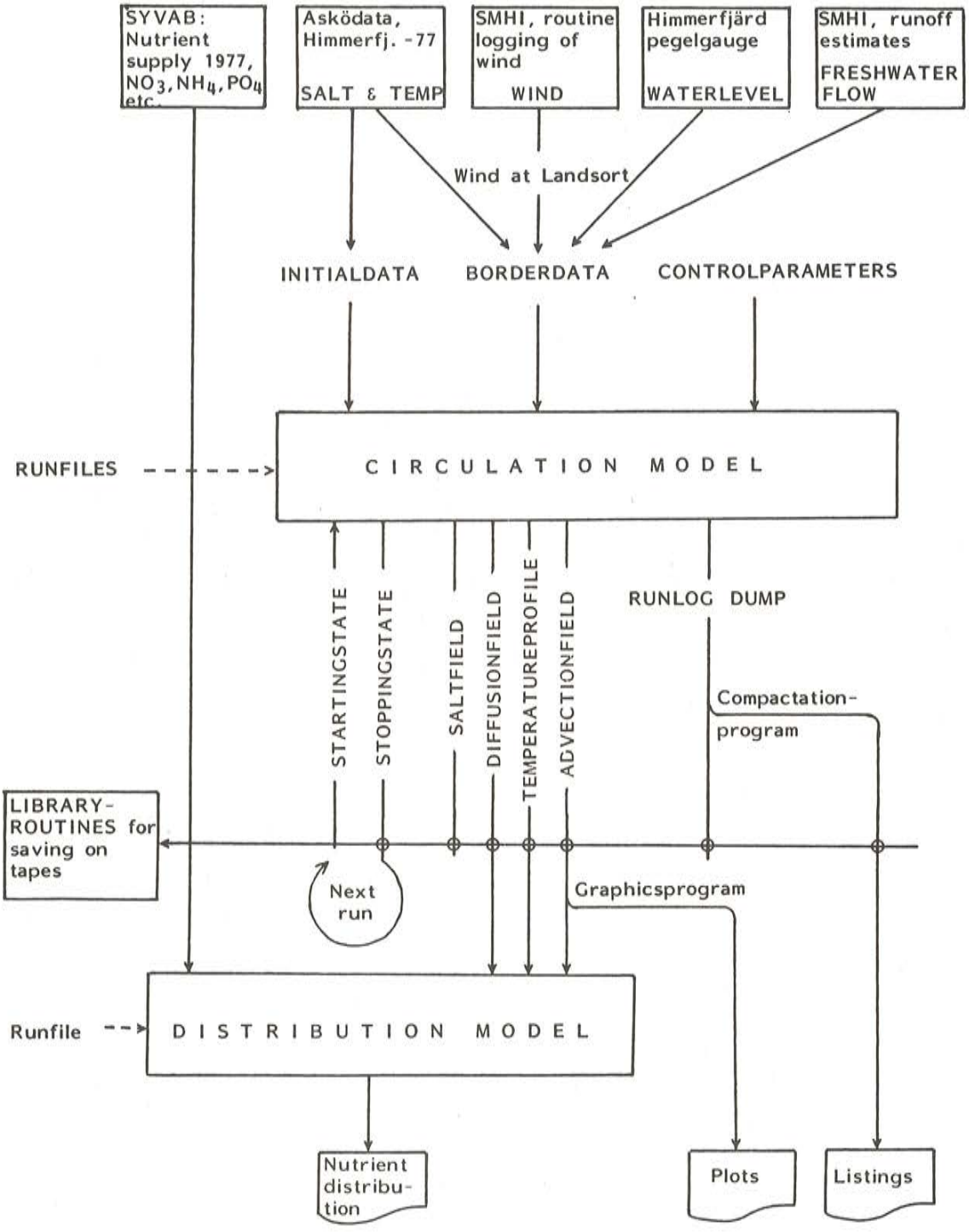

Figure 5. Flow-chart over how the various input and output data for the circulation model relate and how this interfaces to the coming distribution model. The circulation model is designed to be able to stop on command and then be restarted from the same time step, without any loss of continuity. This explains why the stopping state is stored together with the other simulated data.

The eddy viscosity parameters (momentum diffusion) have been assumed to be independent of depth. If the windspeed exceeds a critical limit τ_w^*, then in the model the viscosity parameters are increased in linear proportion to the ratio τ_w/τ_w^*. This is meant to represent the extra turbulence created by wind action when breaking waves are formed and only affects the mixing above a pycnocline.

The ratio between eddy diffusion K_V and eddy viscosity A_V has been investigated in the Baltic by Kullenberg (1971, 1976). His result can be summarized with the following formula which is implemented in the model:

$$\left.\begin{array}{ll} K_V = A_V \cdot 0.1/Ri & \text{if } Ri > 0.1 \\ K_V = A_V & \text{if } Ri < 0.1 \end{array}\right\} \quad (1b)$$

In eq. (1b) R_i denotes the Richardson number:

$$R_i = \frac{g}{\rho}\frac{\partial \rho}{\partial z} \Big/ \left(\frac{\partial u}{\partial z}\right)^2 \quad (1c)$$

Strong shears (high $\partial u/\partial z$ factor) mean increased eddy diffusion, while the existence of a sharp pycnocline (high $\partial \rho/\partial z$ factor) works the other way around.

The diffusion lower layer factor listed in Table 2 makes it possible to reduce the eddy diffusion parameter below the pycnocline. The actual value of τ_w^* is near 12 m/s and is deemed somewhat high for Himmerfjärd. Because a lower value means a lowered eddy viscosity and consequently higher current velocity, the margin for numerical stability would be lessened in inverse squared proportion. This is clearly seen from the Courant-Friedrich-Levy criterion which ensures numerical stability:

$$\Delta t\left(\frac{U_{max}}{\Delta x} + \frac{W_{max}}{\Delta z}\right) < \left[1 - 8\ \Delta t\left(\frac{A_V}{\Delta z^2} + \frac{A_H}{\Delta x^2}\right)\right]^{0.5} \quad (3a)$$

Since the model employs an implicit numerical scheme in the vertical direction, the vertical components in eq. (3a) are irrelevant and the inequivalence reduces to:

$$\Delta t \cdot \frac{U_{max}}{\Delta x} < \left[1 - 8\,\Delta t \cdot \frac{A_H}{\Delta x^2}\right]^{0.5} \qquad (3b)$$

If the highest observed horizontal current does not exceed 1.35 m/s, e.q. (3b) using the model parameters in Table 2 yields $\Delta t < 360$ s. This is the timestep normally used throughout the simulations. The argument has here been somewhat reversed, since computer cost consideration for obvious reasons must limit the value of the critical parameters, the timestep, and the size of the gridnet (Δx=500 m and Δz = 2 m). These latter are fed into the model as scale factors in order to make the model equations non-dimensional (see Appendix I).

5. VALIDATION RUNS

The primary objective to run the model for the time period with existing independently measured and computed data was at the beginning not very promising because numerical instability problems inevitably occurred after 10 days of simulation. The countermeasure was a gradual smoothing of the fjord hypsography. After having transferred the model to the CD170 computer at QZ, it was possible to complete the intended 3-week simulation corresponding to the period 77-09-01 to 77-09-20. The first 24-h period was discarded to permit the initial gravitational baroclinic tensions to be released. A three-dimensional graph of the initial rapid current transition in Skanssund is seen in Figure 6.

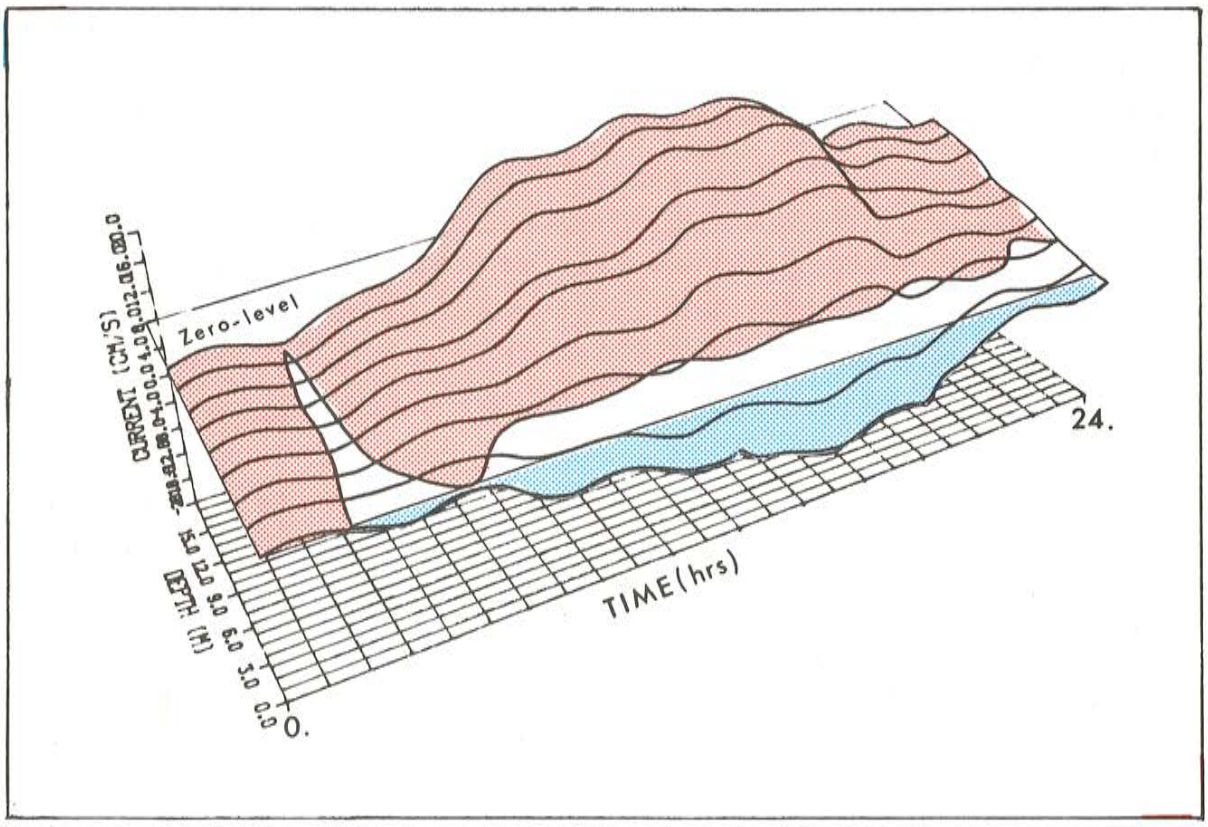

Figure 6. Transitional current through Skanssund as a function of time and depth, as the initial built-in baroclinic field recoils to attain a dynamic equilibrium. A zero-level plane is separating positive currents (red) from negative (blue).

Toll (1980) had calculated the currents in Skanssund and the conjoined Oaxen-Regarn-Koholm sounds, and it seemed appropriate to make the first comparison to these: in Figure 7a and b such a comparison is made. It is to be noted that Toll's calculation is mainly based on diurnal measurements, while the model has a theoretical time resolution of 6 min. Since the wind data are given at 3-h intervals, this is a more appropriate indication of the model's true time-resolving property, yet more frequent by a factor of 8 than the measured data. Consequently there is a higher frequency variation in the simulated data. From Figure 7a and b, the striking similarity in the current pattern can be seen. Even more to the point, the correct order of magnitude of the currents is regenerated, although the model tends to underestimate. It must be kept in mind that the parameters used were directly copied from the Sound (Öresund) application by Svensson and Wilmot (1978). The results were thus very encouraging and the simulation efforts were shifted to trying to understand why and how this could be the case. In order to achieve a statistical measure for the goodness of fit for these simulations, a crude cross-correlation with matching data points for the respective measured and simulated sound currents (current velocities resolved in time x depth) yielded $r = 0.73$. This estimate does not take the similarity of the two patterns of measured and simulated data in Figure 7 into account, which consequence is immediately apparent by ocular inspection.

In the first place it must be noted that the model responded rapidly to wind shifts. In the mid-simulation period (day 14) there was a sudden change from northerly to southerly, which was directly apprehended by the model. This is consistent with the opinion (B. Kjerfve, pers. comm.) that Himmerfjärd is an event-oriented, wind-effect dominated estuary.

The influence of the low-frequency barotropic flow, expressed as water level changes, was examined by reversing the sign of the flow. This altered the flow patterns slightly, to less favorable ones, but their major features remained the same.

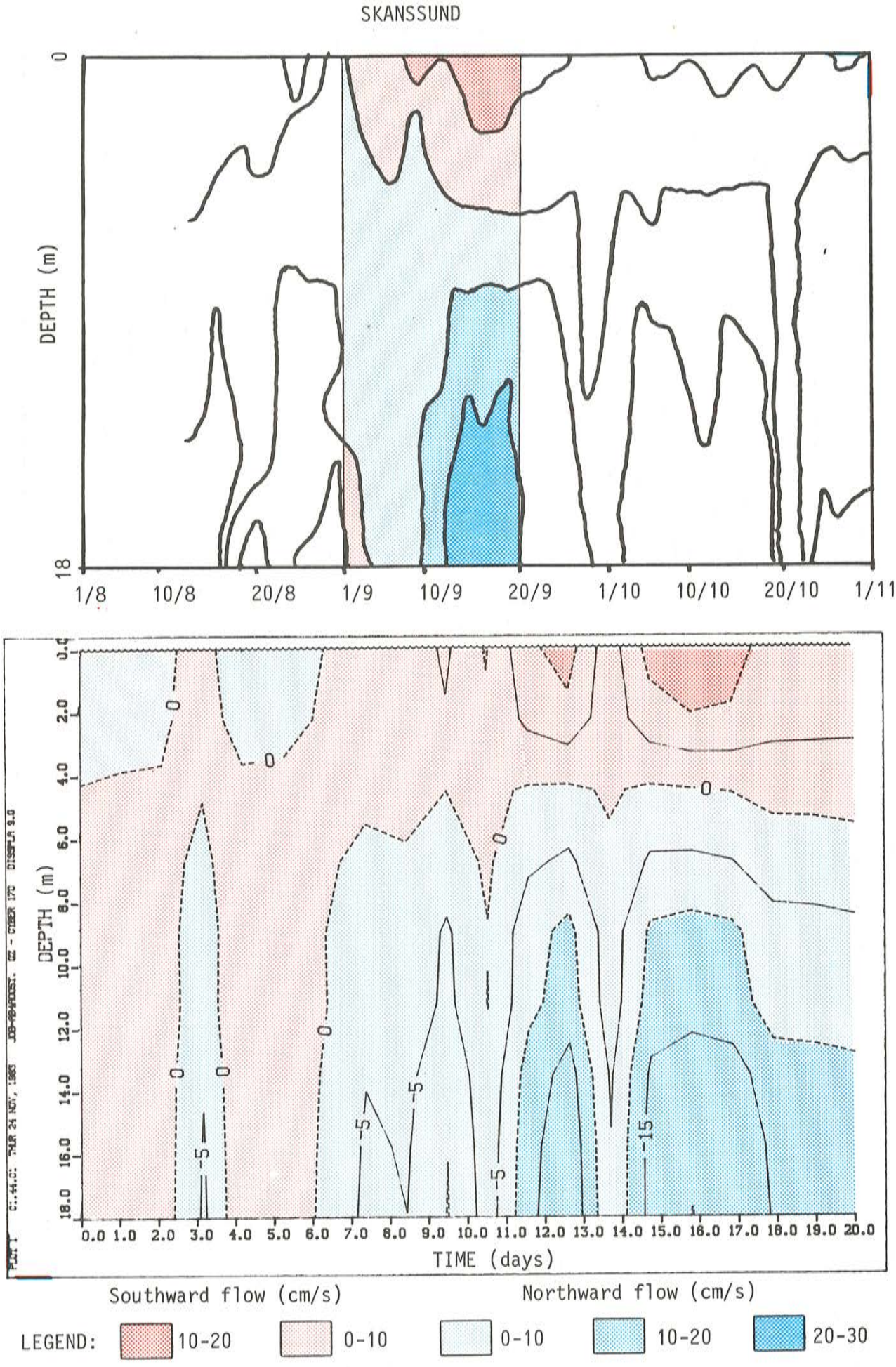

Figure 7 a. Isotachs for measured (upper diagram)* and simulated currents in Skanssund. Only the coinciding part of the upper diagram is marked according to the legend.

---

* After Toll (1980).

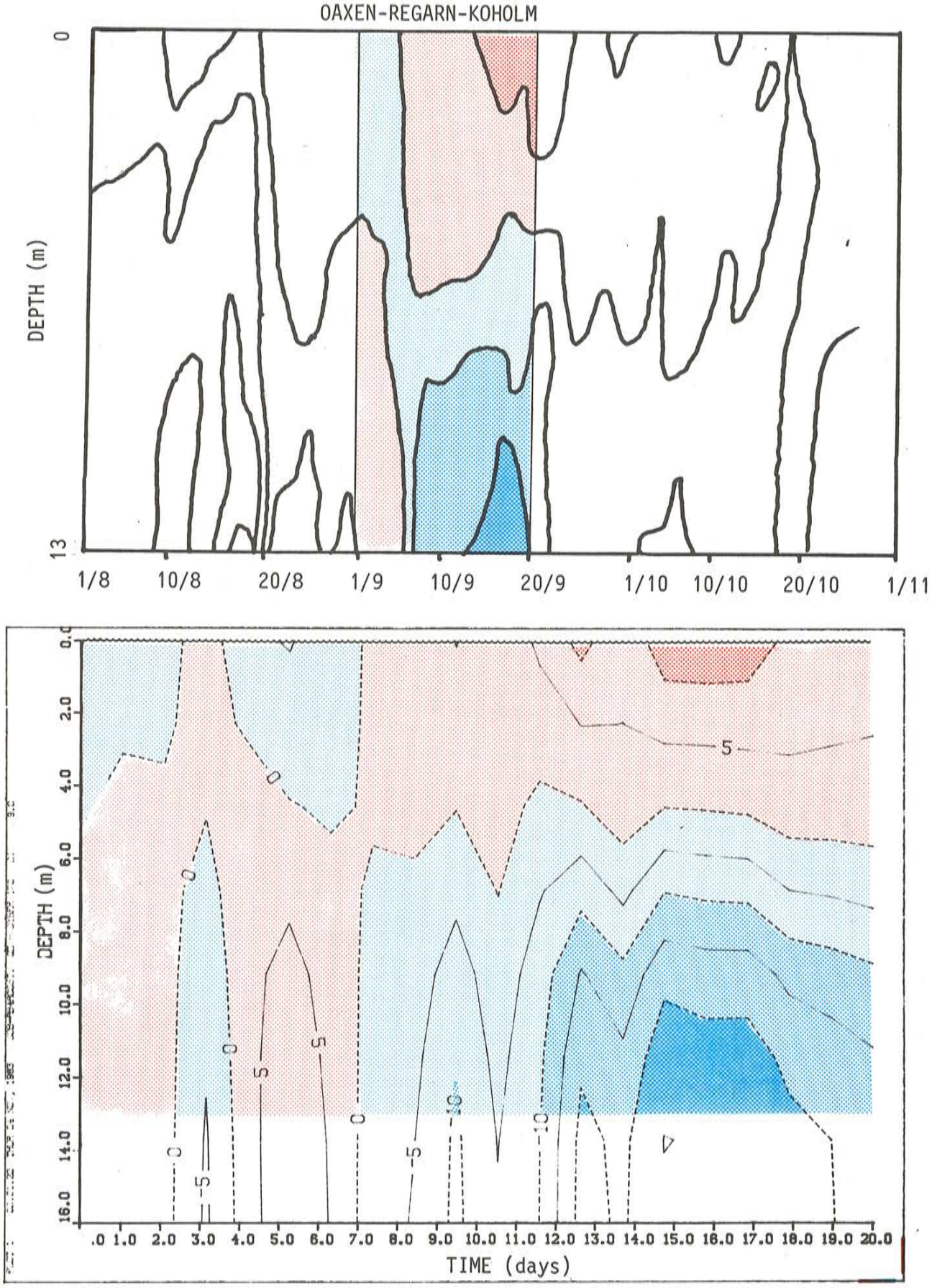

Figure 7 b. Isotachs for measured (upper diagram)* and simulated currents in the conjoined Oaxen-Regarn-Koholm sounds. Only the coinciding part of the upper diagram is marked according to the legend. Contrary to Skanssund this applies not only to the time but to the depth as well.

---

* After Toll (1980).

The fluctuating seiche was switched off and it was confirmed quite convincingly that its direct influence on the water transport was negligible in comparison to other factors. This means that even if it is given the maximum magnitude (100 m^3/s) estimated by Toll (1980), its short period of 4 h only makes the water in the sounds shift back and forth in the oblongated sounds, possibly having its major effect by contributing to the already high turbulence there, and by obstructing the estuarine flow by so-called tidal choking (see chapter 8). It is also convenient to have the seiche as a time mark in the simulations and since it is easier to filter its direct barotropic effect than to superimpose it, it was decided to let it remain switched on. See also section 8.2.

The realism of the estuarine flow caused by the freshwater flow and the influence of changes in the S&T profiles at the border are more difficult to judge because of lack of data. This was evident later when trial runs with a dispersion model were performed with inputted fields, identical to those computed by the simulation model, but at a less frequent periodicity of 1 h compared to the simulation time-step of 6 min. At least the vertical mixing of S&T was found to be much too high. This could have been expected from the discussion in the previous chapter. Again, it does not seem justified to increase the stability-limiting horizontal eddy viscosity parameter (A_H) only for the sake of stability. To keep it as close to the measured value (Buch, 1980) seemed more advisable, even if this means tolerating the high value of the vertical eddy diffusivity, K_v, responsible for the unrealisticaly high vertical mixing observed here and in other dispersal simulations. This is provided that A_v and K_v should be of the same order of magnitude which is physically plausible with the correction Kullenberg's formula prescribes, since the same turbulent process is responsible for the diffusion of both momentum and the S&T-fields. Thus a lowered value in K_v means a lower A_v, yielding a slower vertical momentum diffusion. This leads to the result that at local points, mainly narrowing

sections near the sounds, the probability increases that the stability criterion eq. (3b) is no longer met. This is due to the occurrence of high horizontal currents which would be diffused away in the vertical for a higher A_v value. A way out of this predicament is of course to use a shorter timestep, though this possibility was not availabe in this study for economical reasons.

In order to compare the water transports in the sound, the down- and up-estuarine flows were calculated. As can be seen from Figure 8a, their difference gives the net flow composed by the water level change and the seiche. Since the influence of

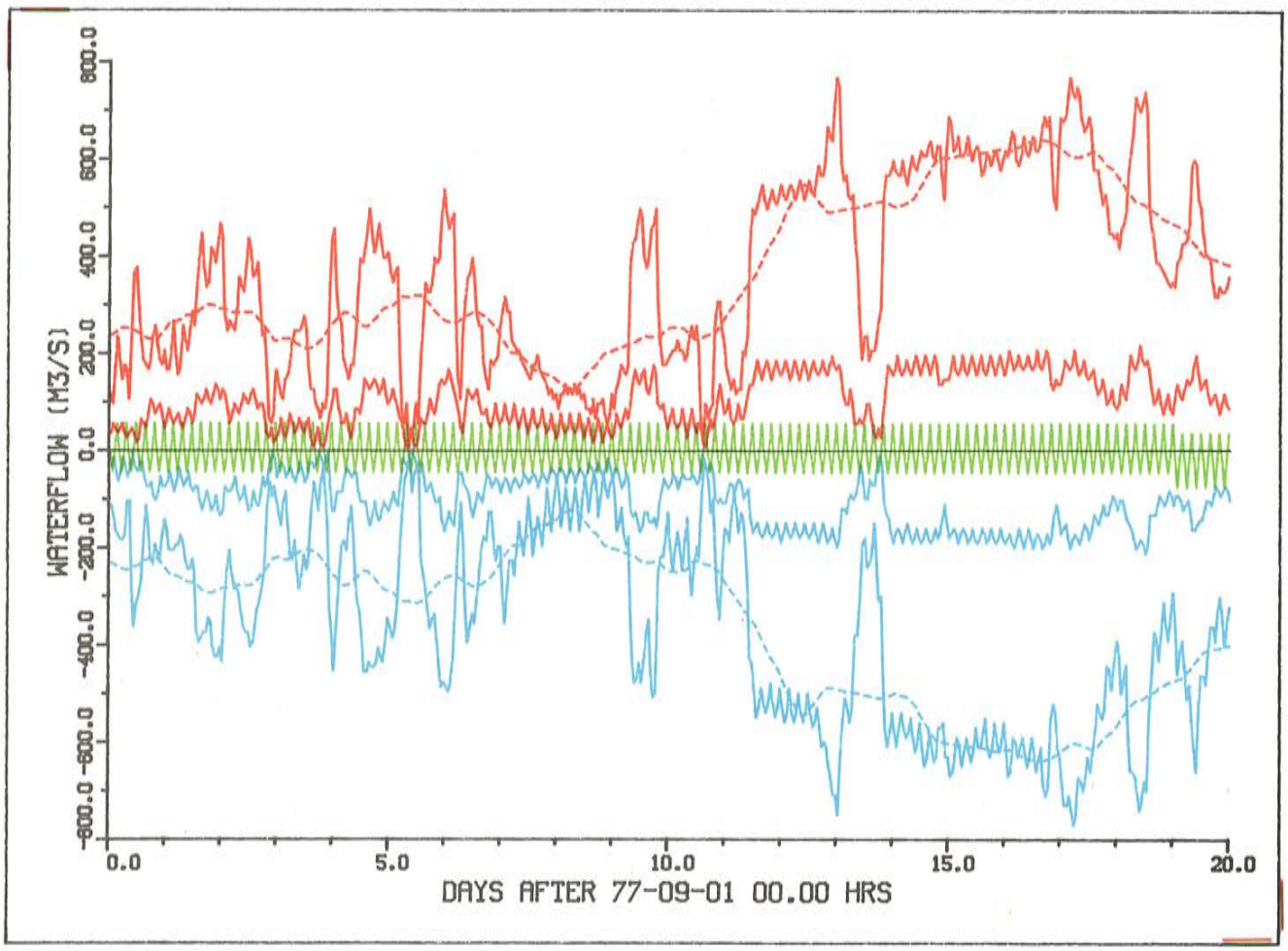

Figure 8 a. The red curves show incoming water filling the inner basin of Himmerfjärd and the blue ones outgoing water. Their difference (green curve) is therefore the two barotropic components due to water level changes and the net seiche contribution, summed over the SS and the ORK sounds. The largest of the two respective solid lines of either color represents the total filling flow, while the smaller shows the contribution of SS. The broken lines give a three-day running average of the total flow.

these is minor, a more practical way to depict these is to compute the surface flow down to a point where the current changes direction. This is shown in Figure 8b, where transport data calculated by Toll (1980) also are included. When comparing the simulated surface flow-data with the measured, three remarks can immediately be made. The first is the aberration of the mean current level (broken line in Figure 8b) that is largest for the Skanssund and of order of 100 m^3/s. This corresponds to about 6 cm/s velocity, using half-of-sound transect area. The discrepancy is thus detectable with the current measurement method used, i.e. gelantine prisms. A quite reasonable explanation is, though, that when computing the

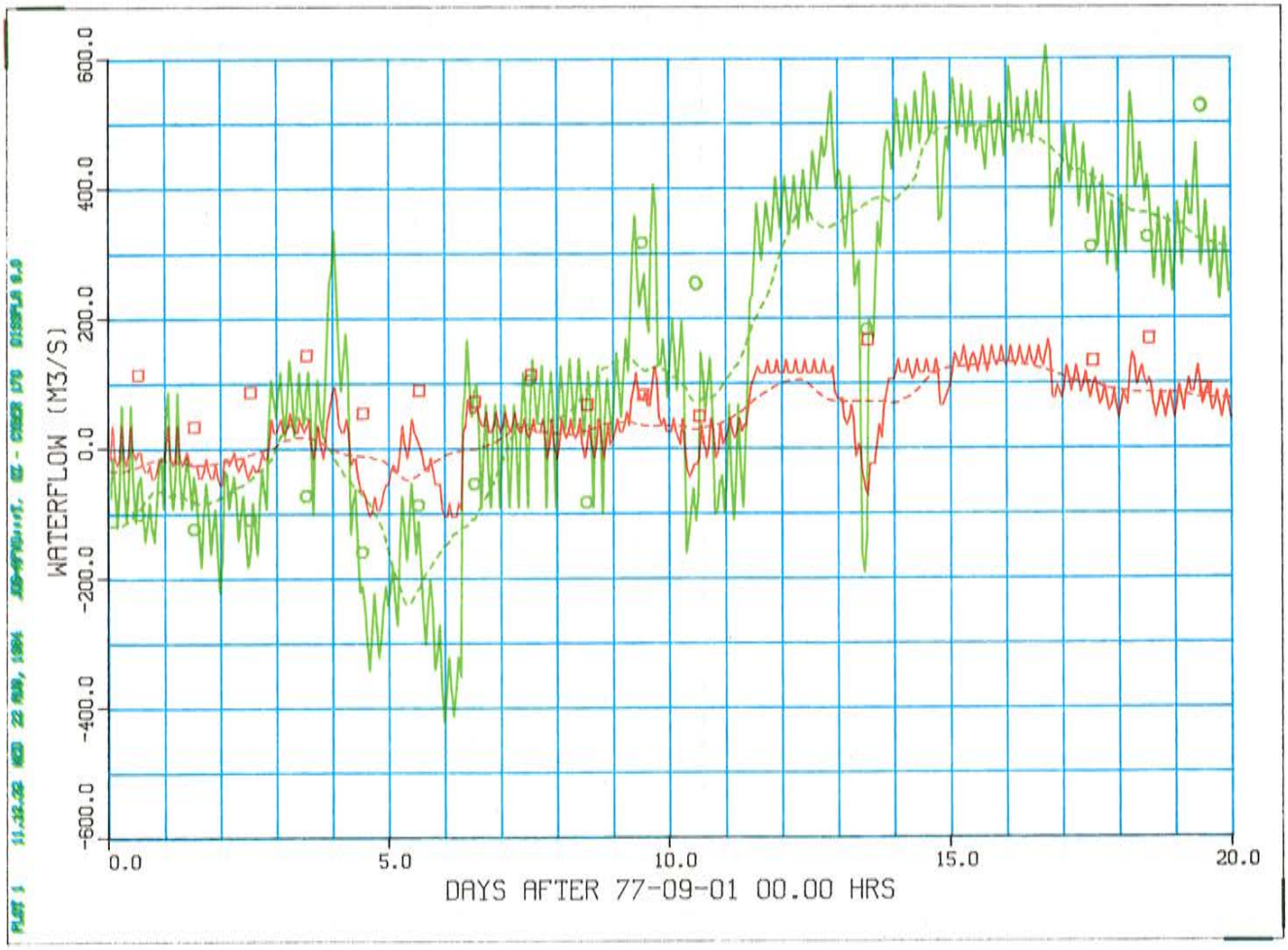

Figure 8 b. The same data as in Figure 8 a are here presented differently. The green curve now denotes *the surface flow of ORK sounds, integrated down to the depth where the current reverses*, i.e. changes sign. The red curve for SS is defined analogously. This convention (including color code) will be kept consistent in the following figures and exceptions will be pointed out. Corresponding measurement-based surface transports, computed by Toll (1980), are denoted by green circles for ORK and by red squares for SS. For comments on the fit between these data, see text.

transports, Toll's scheme involved deviant surface areas, compared to the ones listed in Table 2. He first compensated the measured current in each sound with a barotropic flow, to achieve a net water balance for the inner basin. On these current profiles he superimposed an additional barotropic flow to make up for the observed water level change. His superimposed barotropic compensational flows thus can well explain the observed difference. The second remark is that during periods of strong wind surges measurements were not performed. This is most unfortunate from a validation point of view, but understandable from that of the personnel who were carrying out the measurements in small boats.

Third and last, it is interesting to note that the ripple caused by the superimposed seiche for the ORK sounds covers the measured data points for the upper layer unaveraged flows surprisingly well. However the measurements were not taken exactly at noon as indicated in the figure, but had a scatter of about $\mp$ 2 h. Not being entirely simultaneous, unfortunate

combinations of the different sound measurements could possibly explain the otherwise inexplainable discrepancy at day 10.

These remarks do not much tarnish the lasting conclusion that there exists an astonishingly good fit between the simulated and the computed data from measurements for the validation period. The model thus convincingly well reflects the dominating mechanisms involved for the water turnover and its validity for simulation of other parts of the year could be at least hoped for, if not trusted.

6. SEASONAL CASE STUDIES

After the primary objective of validation had been accomplished, the secondary goal to estimate a yearly water turnover was begun. In the first place, this entails determining how well the model performs during other times of the year. A number of representative 3-week periods, each

corresponding to a typical seasonal flow pattern, had to be selected over the biological year. The following were chosen:

1. Winter situation with ice cover;
2. a. Spring bloom;
   b. Spring flood;
3. Summer stratification;
4. Fall isothermal situation.

A priori these periods would cover the principal modes under which the water moves in the Himmerfjärd estuary, provided that the wind influence is also representative. In Figure 9a, the chosen periods çan be related to the wind at Landsort shown as a running 3-day average.

The actual choice of the exact starting dates was, of course, decided to correspond to the Askö data sampling dates, except

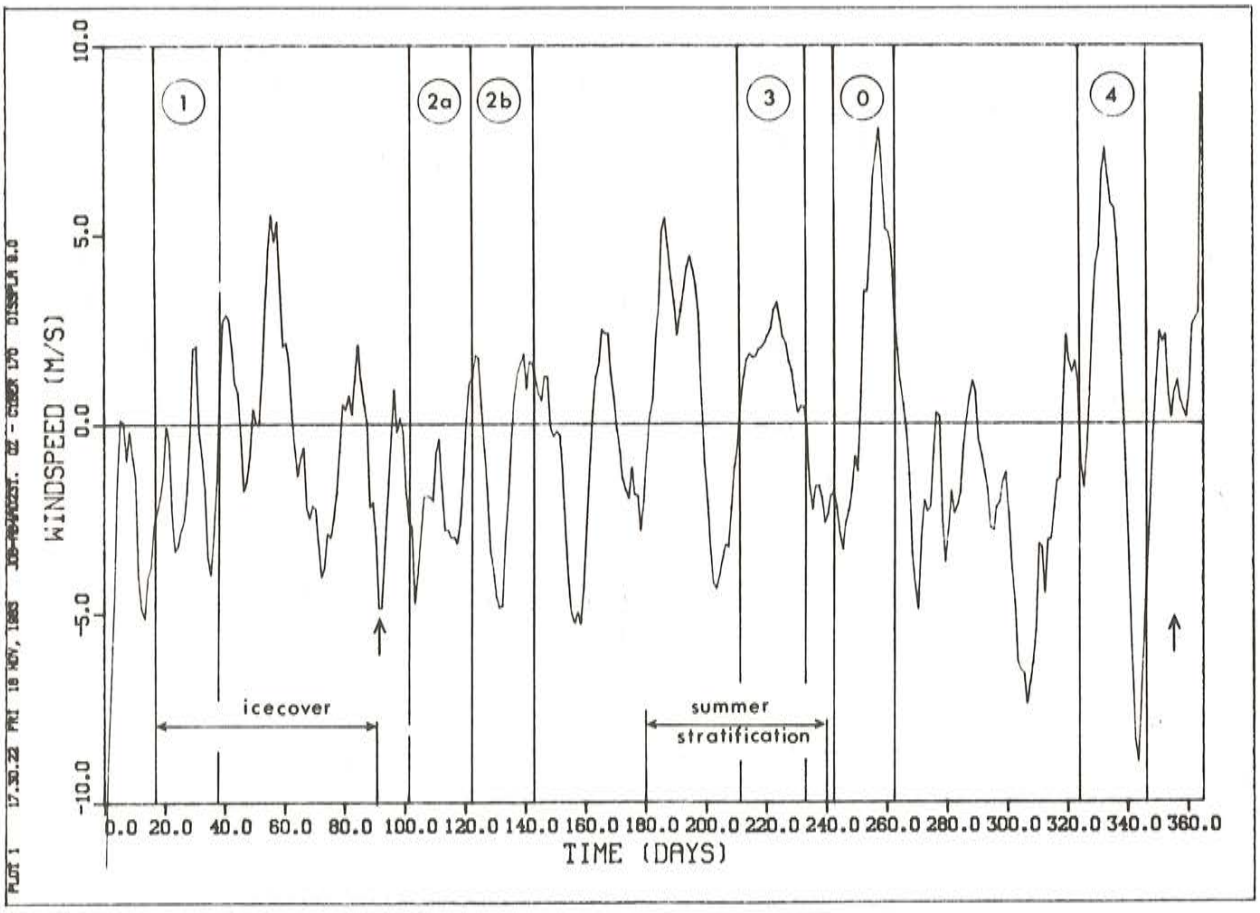

Figure 9 a. The wind (N/S-component) at Landsort shown as a running 3-day average for 1977. The choice of the various seasons can be seen as can the duration of the other relevant conditions affecting the circulation. The arrows indicate the vernal and autumnal total mixing events. Northerly wind is given positive sign.

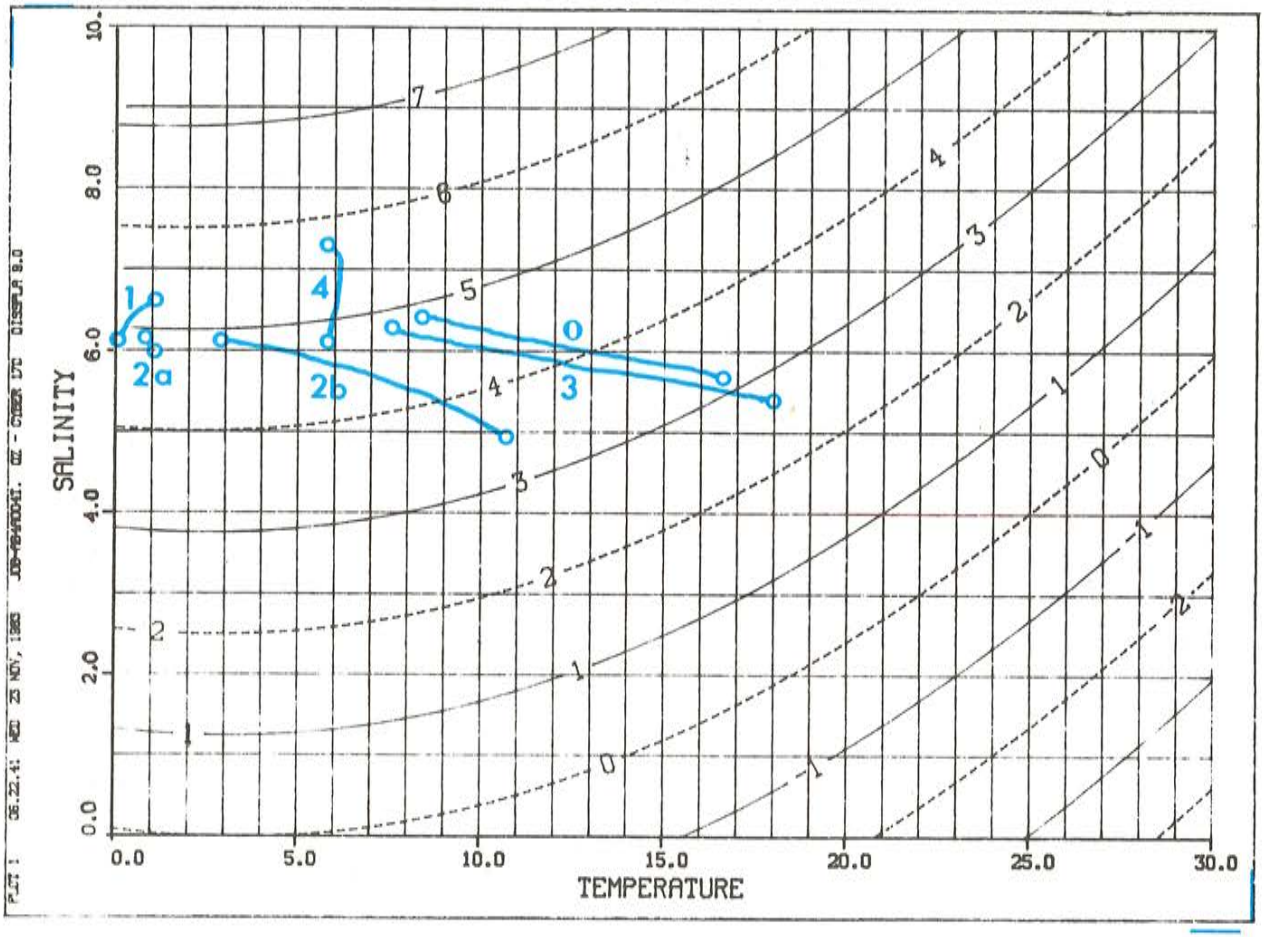

Figure 9 b Salinity and temperature loci for the Himmerfjärd water at the beginning of the respective seasons with depth as parameter, used for the initial filling of the model. These data are computed as the average of the inner basin sample stations (station 3 an 4 in Figure 1) but the difference in comparison to the border data is in general negligible.

for 2b that followed directly after 2a, using the latter's terminal fields as initial data, i.e. the normal procedure when continuing a simulation. The spring flood was a unique occasion in 1977 when a considerably increased amount of Lake Mälar water was flushed down Himmerfjärd and not (as the verdict of the Swedish water tribunal prescribes) through the Stockholm archipelago. This meant a quadrupled amount of freshwater flow from the normal 10 m^3/s to a peak at about 40 m^3/s for a period of about three weeks.

To make these simulations, renewed data gathering had to be undertaken. This could now be achieved much more efficiently since the model's sensitivity to various input data was now better understood. For instance were the initial fields provided homogenously with respect to the fjordwise axis.

In Figure 9b the vertical distribution of S&T data with respect

to depth for the different periods is plotted. The validation period was included in this list of simulations as a control to make sure input data were correctly processed, and is referred to as number 0 in Figure 8 and in the following. Prior to the seasonal runs a slight revision of the parameters (see Table 2) and the topography (mainly of the sounds) was undertaken. It was ascertained that the surface transports compared to measurement data were not inferior to the results of the validation run. From a modelling point of view this is a calibration measure, justified since it primarily affected the transport quantities, not the flow patterns, depicted in Figure 7a and b which was thoroughly checked. Thus the differences that can be observed when comparing the output of this run (Figure 10) with the earlier validation data (Figure 8b) are minute for the ORK sounds; for SS the fit with the

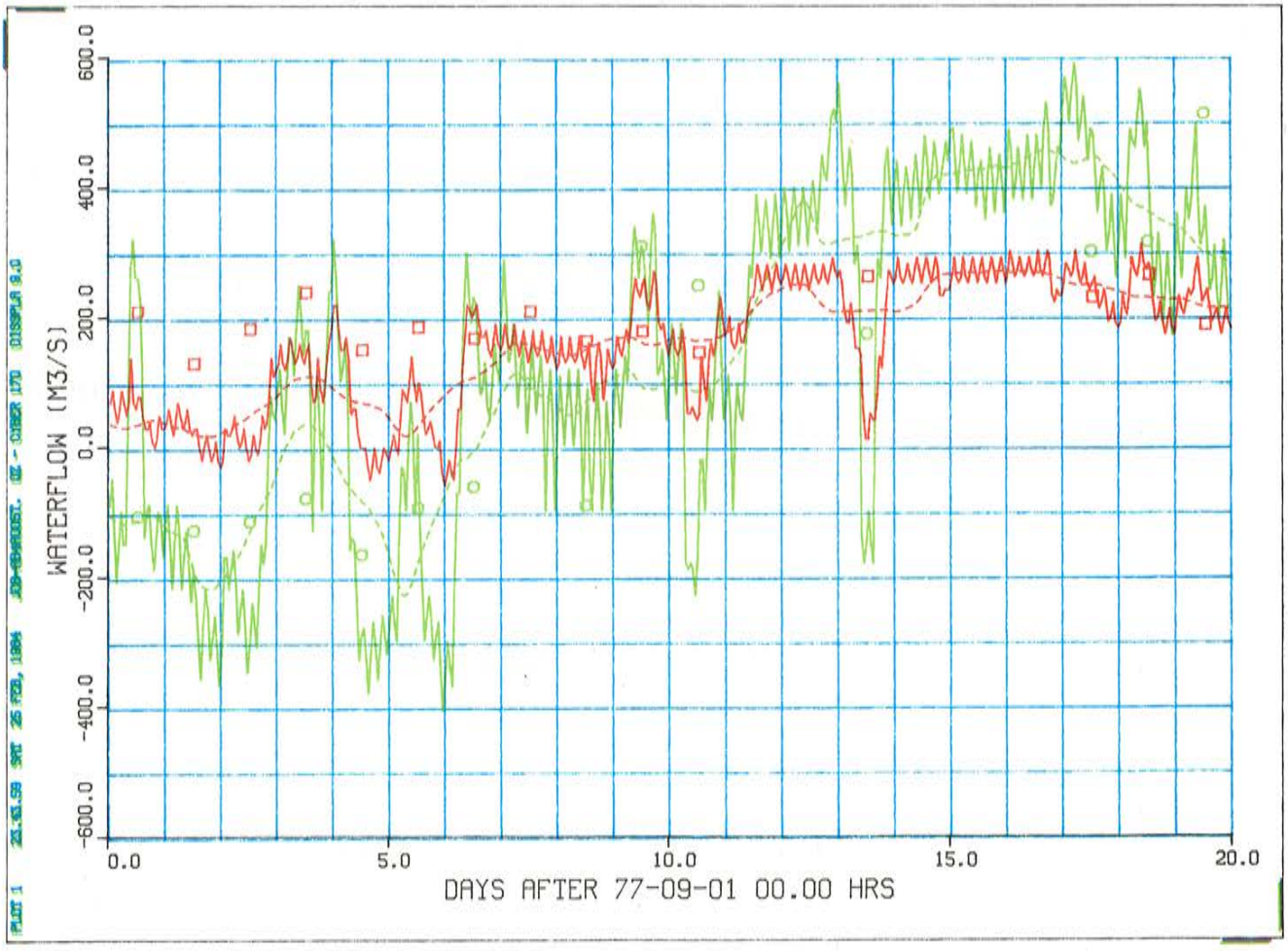

Figure 10. Test run for the validation period with new set of parameters pertaining to vertical eddy viscosity and diffusivity properties. The fit to the measurement-based data (rings and squares) is somewhat improved due to calibration. Compare Figure 8 b.

observed data is less convincing for the first 10 days but improved for the last half of the period. An account of the various seasonal flow modes and how well the model deals with them follows.

Without exception, all the following simulations were run with the same set of parameters, listed in Table 2. For the initial transient 24-h period the vertical eddy viscosity parameter was set to 50 cm^2/s in order to avoid numerical instability as well as to speed up the built-in baroclinic forces to stabilize the S&T fields when starting to move water around.

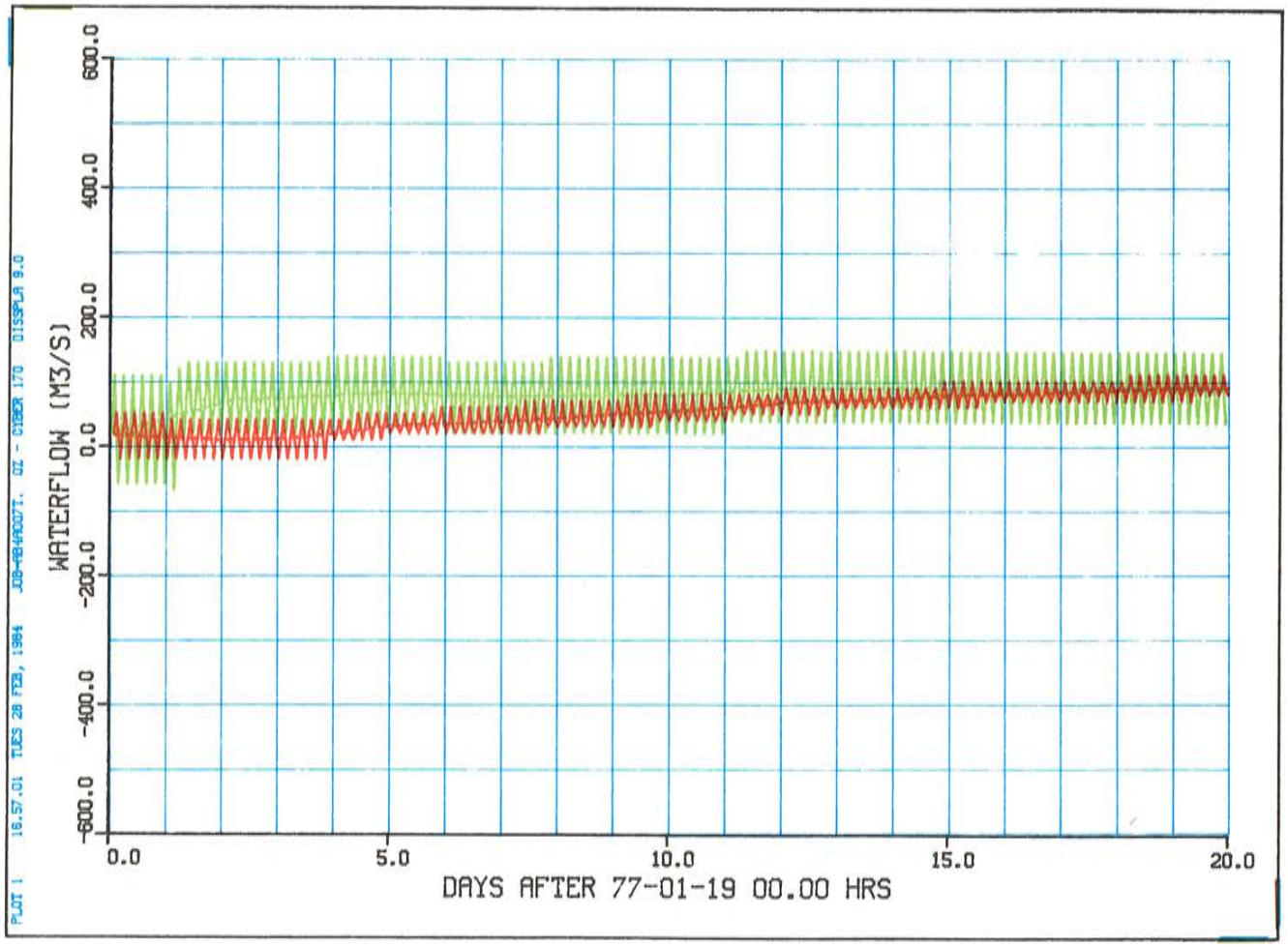

Figure 11. Ice period (#1) simulation. Both the SS and ORK transport reach the level of ca. 90. m^3/s. This is very likely an unrealistically high level. For discussion, see text, in particular Chapter 8.2.

6.1 Winter situation with ice cover

According to Figure 9b, during winter the S&T fields are quite homogenous. From Figure 11 it can be seen how the estuarine flow gradually increases to reach about 90 m^3/s at the end of the period for both SS and ORK sounds. For the latter sounds this seems reasonable. The only known actual current measurement under the ice cover in Himmerfjärd was undertaken in January 1983. At Uddsund and Regarn-Koholm sounds the measurements then gave us a result that currents were below the detection level of about 1 cm/s at all depths. For the ORK sounds this level corresponds to a flow of the same order of magnitude as the simulated one; consequently for these conjoined sounds there is no contradiction between measured and simulated data when the wind forcing is ruled out and the estuarine freshwater flow is the only forcing apart from the barotropic water level changes including the seiche.

On the other hand, the estuarine circulation for the Skanssund seems much too high (A. Stigebrandt, pers. comm.), considering that the wind influence is null. Compare Section 6.2 below. It is not certain that the fjords north of Skanssund in fact were frozen when Himmerfjärd was so. In any case, the ferry personnel state (L. Andersson, pers. comm.) that the currents in Skanssund can easily be several knots even when the ice coverage reaches its maximum. The conclusion must be that although part of the simulated flow could possibly be explained by mixing energy provided by turbulence in the narrow fjords taking the place of wind mixing (Hamilton and Rattray, 1978), the simulated estuarine flow is probably much too high under the circumstances. This is a warning that corrective measures must be taken when simulating the winter situation.

6.2 Spring bloom and flood period

At the starting date of the spring bloom period the vertical density distribution is even more homogenous than for the previous ice period. See curve 2a in Figure 9a. This is because the vernal total mixing event (when this brackish water reaches

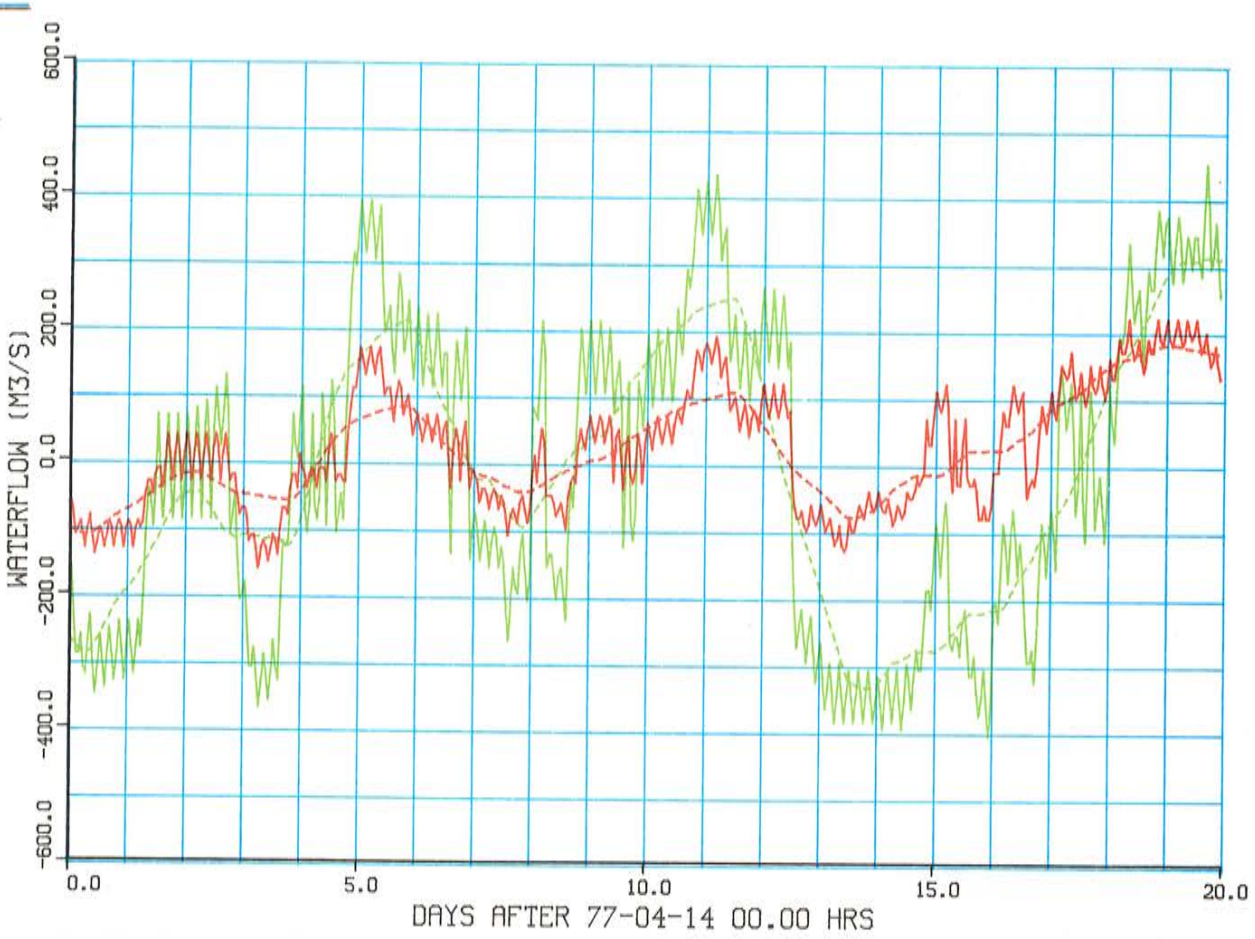

Figure 12 a. Spring bloom period (#2a) simulation. The wind forcing now applies to full effect. The water is still densometrically homogenous since the vernal mixing event is just a few days off.

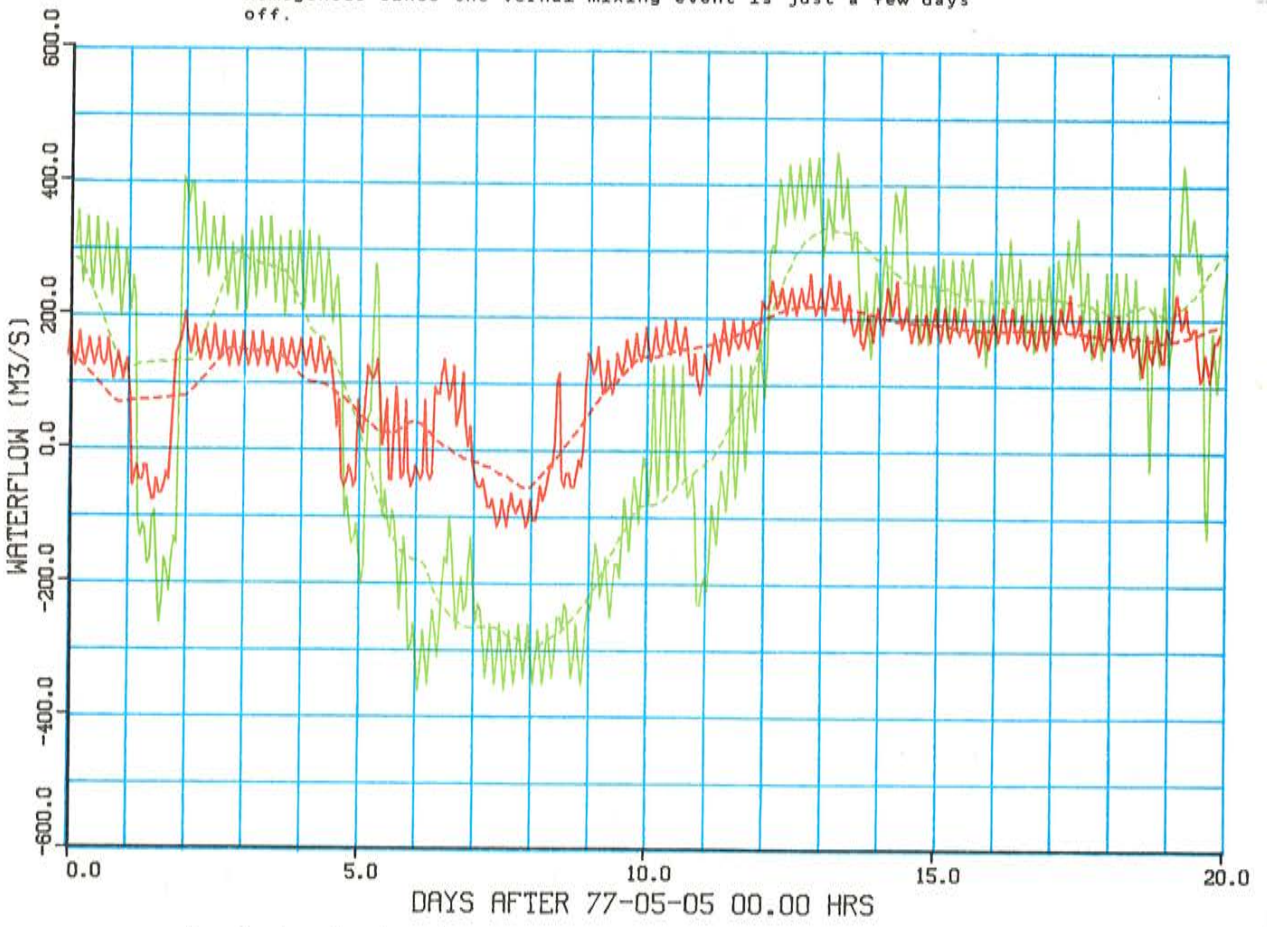

b. Spring flood period (#2b) simulation. The fresh water river flow was increased from 10 m^3/s to 40 m^3/s during this period that followed immediately after the previous one (#2a). The purpose of including this period was to test the model's realism in simulating the esuarine flow component.

its maximum density) has just taken place. The water heats rapidly, and by the end of the 3-week period it has the distribution according to curve 2b, the starting point of spring flood period. The simplest possible heating mechanism is included in the model in that the virtual uppermost horizontal gridpoints are forced to directly attain the measured surface temperature. The vertical mixing then distributes the absorbed thermal energy downwards.

The freshwater flow remained at 10 m^3/s during most of the 2a-simulation but was then gradually increased to peak at 40 m^3/s for almost the entire 2b-simulation. The expected consequences for the estuarine flow are discussed in Section 8.2. The residence time of the freshwater is given by Stigebrandt (1981):

$$\tau_f = A(g\ S_2\ B_m^2)^{-1/3}\ Q_f^{-1/3} \qquad (4)$$

The time it will take for the estuary to respond to a change in Q_f will be of the same order of magnitude. Q_f = 10 m^3/s gives τ_f = 18 days, while Q_f = 40 m^3/s shortens this to 11 days. Steady-state would theoretically have been established for the Skanssund flow provided that the wind effect had been restricted to mere mixing.

Since the barotropic flow induced by wind drag cannot be neglected by any means, it is not possible to state other than the simulated transports for Skanssund are compatible with the cited theory based on physical parameters. For the ORK simulations it is more difficult to even check this compatibility since the conjoined area of these sounds is probably too large to establish the dynamic control prescribed by the theory.

6.3 Summer stratification

The most striking feature of the summer stratification simulation (Figure 13) is that the flow in the ORK sounds has

its highest peaks - over 600 m^3/s - even though the windspeed is moderate during the entire period. This is likely to be a reflection of the higher horizontal mobility of water when stratified in layers. The prevailing northerly wind for this period pushes the surface water in both sounds southwards at a fairly steady rate of approximately 100 m^3/s for Skanssund and 300 m^3/s for the ORK sounds. The running 3-day average curve fluctuates, however slowly, about 100 m^3/s from this level for the latter curve.

6.4 Fall isothermal situation

For this period the thermic equilization is clearly seen in Figure 9a. The fjord remained gently stratified with respect to a slightly increasing salinity with depth. During this period a couple of rapid windshifts (N/S component) took place. Even

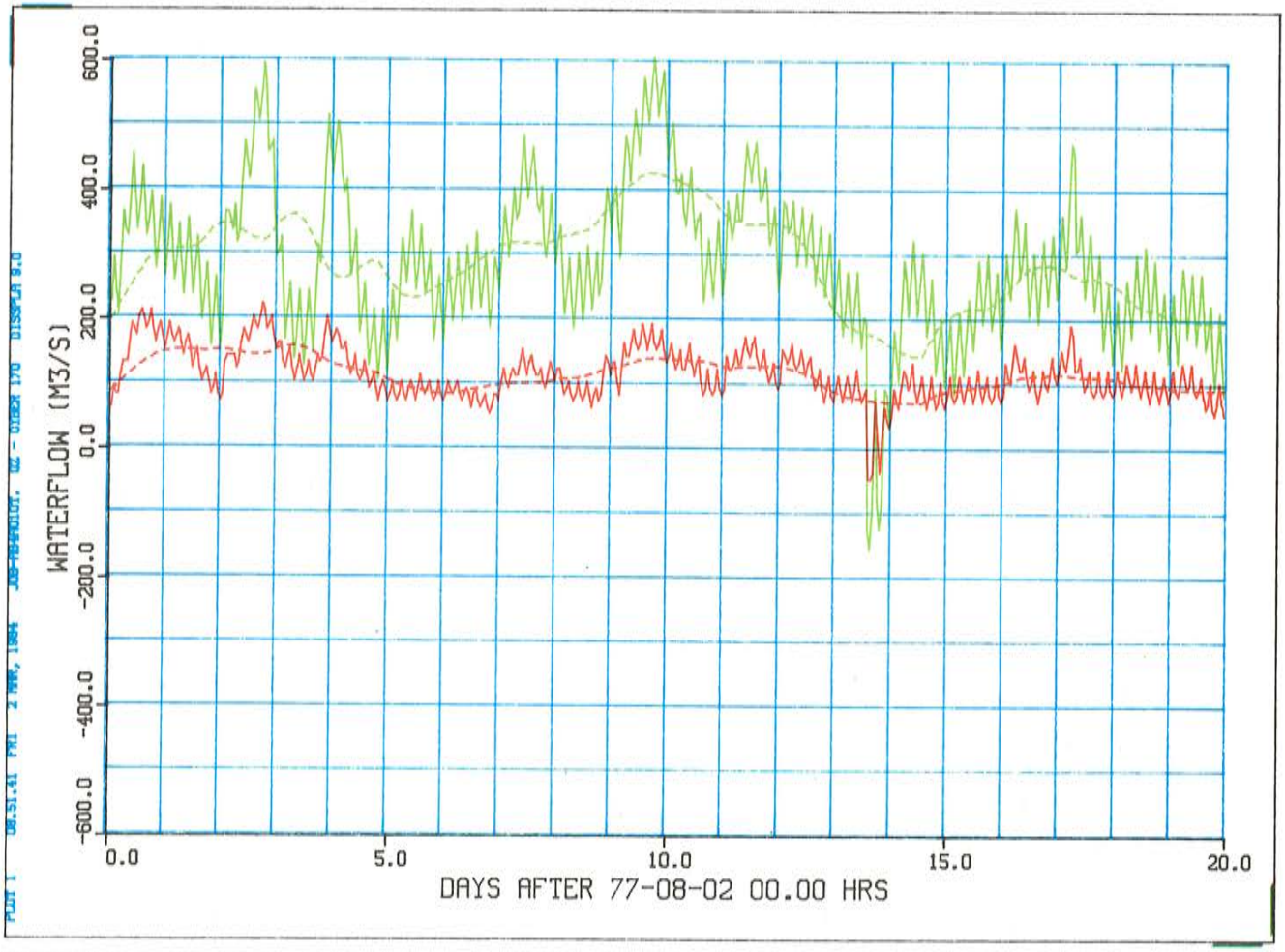

Figure 13. Summer stratification period (#3b) simulation. This period is characterized by its predominating northerly winds, forcing the surface water southwards.

though their respective magnitudes seem different in Figure 9 because of the averaged presentation, in fact they are comparable in magnitude. The resulting fast change in the water transport can be seen in Figure 14. It could be expected that these shifts would cause numerical instabilities, but this was not the case.

Short of field measurements, it is of course a delicate task to make statements of the validity of simulations, both for this one and the previous ones. On the few points, however, where the model can be checked - except for the ice cover period - it cannot be falsified. Therefore it seems plausible that these curves for their respective periods are an approximately correct estimate of the water transport. An overview of the result of these seasonal simulations is given in Figure 15.

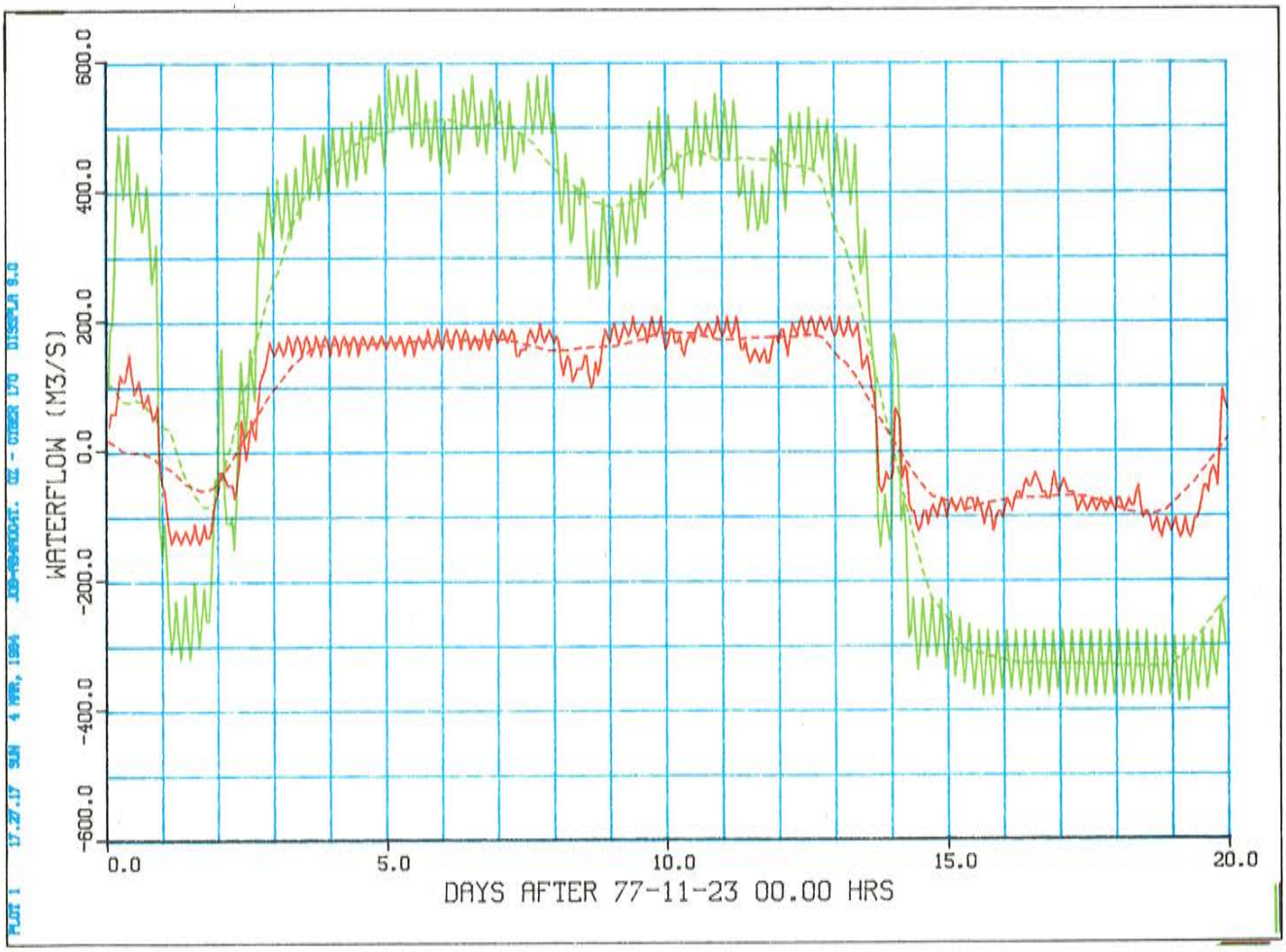

Figure 14. Fall isothermal period (#4) simulation. This period involves the most rapid windshift that was recorded 1977. The flows through the sounds are near the model's maximum transport capacity.

7. WIND PULSE RESPONSES

Since the validation runs clearly established the vast effect of the N/S component of the wind forcing, it seemed interesting to perform a closer study of its influence on the water transport through the sounds. This is the most interesting property concerning the water turnover for a whole-bay budget.

The idea was to force the Himmerfjärd with only wind pulses of various duration and amplitude in addition to the estuarine circulation, driven by Q_f = 10 m^2/s, and to see what relation could be found between these variables. If a reasonably simple and approximately linear such relationship could be found, this would mean an opportunity to achieve the whole-year water turnover objective without having to simulate more than the few

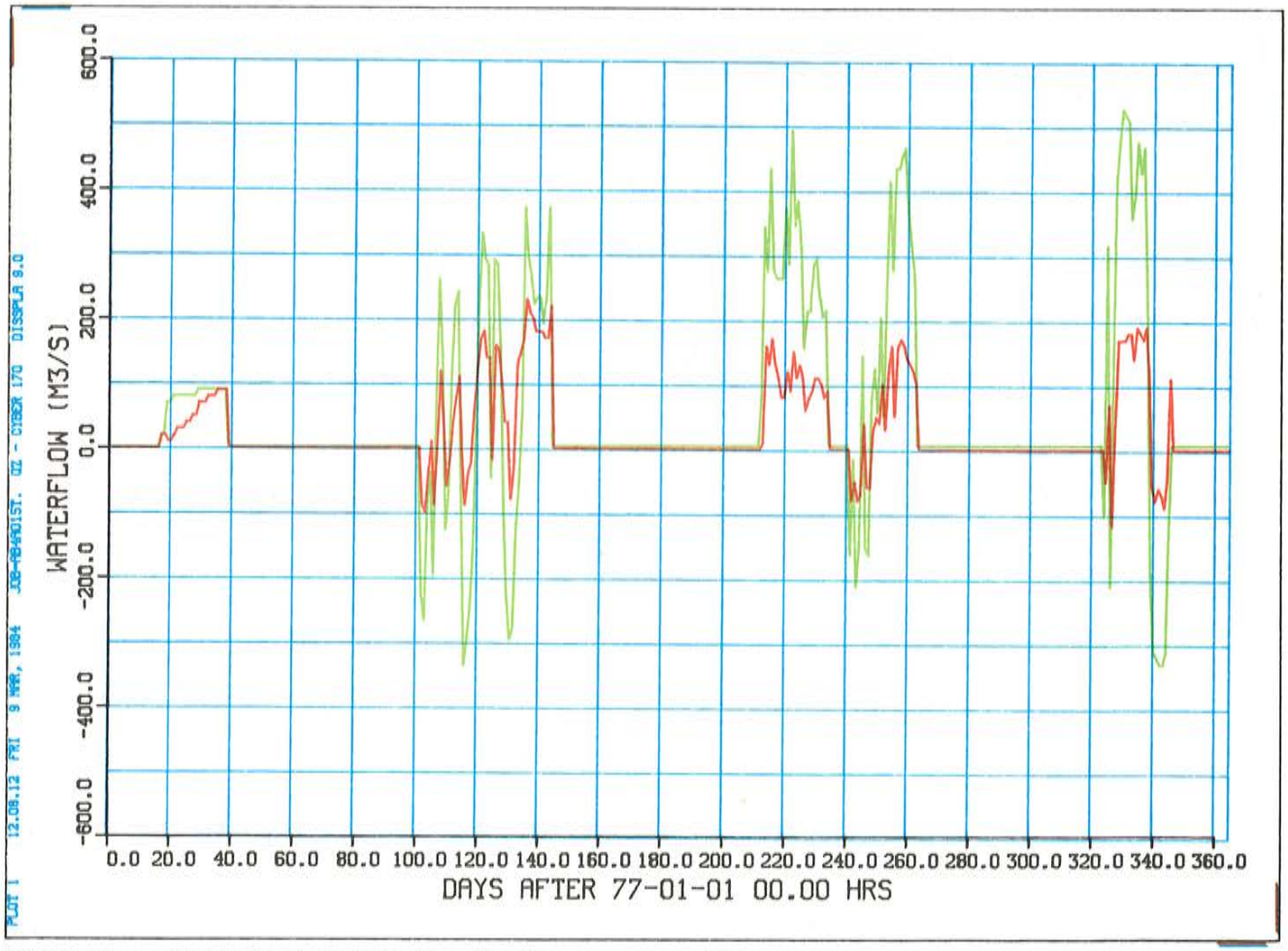

Figure 15. Overview of Figures 10 - 14. The curves are filtered by a 24 h running average and the gaps between the simulation periods are set to zero.

various representative runs described in the previous chapter and then calculate the wind-driven transport as a pulse-response convolution integral.

The results of these attempts were very discouraging. A typical response can be seen from Figure 16, where a wind pulse of 10 m/s with a 12-h duration gives for Skanssund a reasonable response: on the estuarine flow is superimposed a transport pulse with a transient tail that seemingly asymptotically converges towards the undisturbed estuarine circulation flow. This response does not contradict the feasibility of a linear pulse-response analysis of the related kind, but the other curve for Oaxen-Regarn-Koholm does. The interpretation of this latter curve is that the wind builds up a baroclinic field

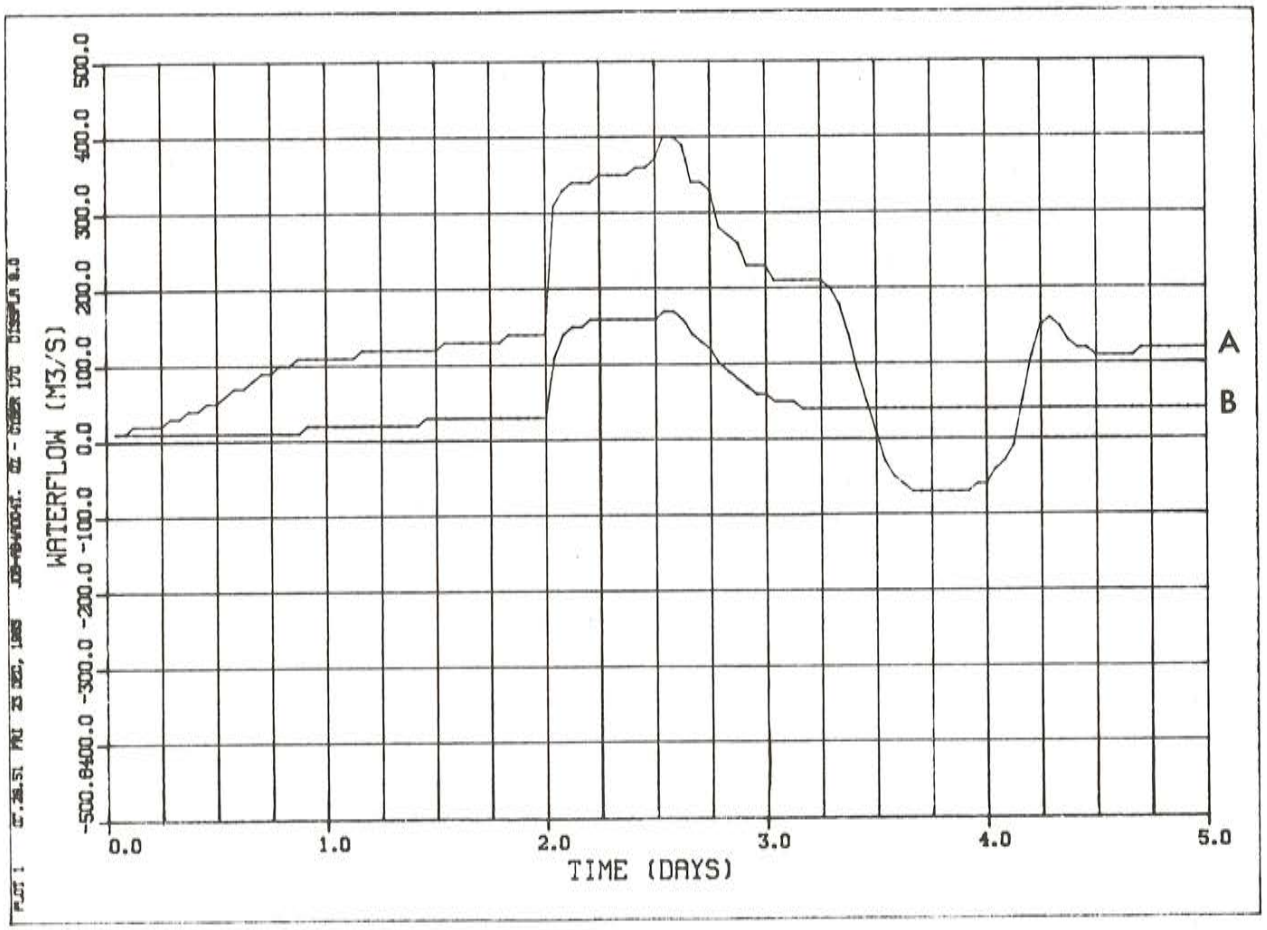

Figure 16. A wind pulse develops 2 days after the model is initialized and lasts for 12 h. The response according to curve (B) is coherent with an assumed linear behavior. The curve (A) on the other hand, backlashes the flow after the duration of the wind pulse, to the extent that the recoiling baroclinic force even reverses the depicted surface flows. The effect of the estuarine forcing (10 m^3/s freshwater) is retained at the end of simulation.

during the wind pulse. This field then recoils and an almost equal amount of water flows back. Other simulations prove that there is a breakpoint (as would be expected) between these two distinct responses. The conclusion follows that any attempt to perform wind pulse analysis by means of linear assumptions must fail by being oversimplistic.

Even if the pulse analysis method for estimating the full-year turnover had to be abandoned, a benefit of these simulations was the detection of a less advantageous trait of the model. During an intensive wind surge exceeding the wind mixing vorticity limit level in Kullenberg's formula, the model responded by increasing the eddy viscosity and the eddy diffusivity parameters, reflecting the increased induced mixing. When the windspeed is returned to zero level after the pulse has elapsed, the kinematic forces will act upon less eddy-viscous water. This means larger horizontal current velocities, in particular at narrowing parts of sounds. From a simulating point of view, the consequence will be that the Courant-Friedrich-Levy stability criterion eq. (3) is no longer met and the program is designed to halt. The remedy for this would be to let apply for the time it takes to allow the wind-enhanced kinematic energy to dissipate into heat by bottom drag friction work, or still better, to let the different viscosity values be gradually transformed into each other. To implement this for future simulations seems well motivated since it also better reflects the physical mechanisms involved.

8. WHOLE-YEAR TURNOVER ESTIMATION

The objective at this point would be to fill in the blank part of the curves between the simulation periods in Figure 15. To do this one must make reasonable assumptions on how the different flows depend on the forcing data known for the whole year, i.e. windspeed, water level changes and freshwater flow. The scheme would be to estimate the water level flow Q_{wl}, and the estuarine flow, Q_e, subtract these and then investigate how the remaining component that would be the wind-driven flow,

Q_w, correlates with the wind for the simulation periods. The seiche is assumed to be filtered away, given a sufficiently long time interval for averaging. An interval of 24 h seems to be the shortest that is still relevant and allows averaging over six seiche periods. If longer intervals seem more appropriate in the future, new averages can easily be formed.

8.1 Water level estimation

It is an easy task to translate the piecewise approximation to a time series of the water level changes' related flow $Q_{wl}(t)$; the results is given in Table 3. The piece-linear approximation can of course be done in various ways, depending on what goodness of fit measure is used. It is to be expected, however, that the different ways to linearize are not critical, as long as the low-frequency behavior coincides reasonably well with measured data. Care has been taken to make certain that the linear sections during the simulation periods are the ones actually used by the model.

8.2 Estuarine circulation

Ideally all gravitationally driven two-layer flows in estuaries are dynamically controlled by a condition, originally given by Stommel and Farmer (1953):

$$F_{d1}^2 + F_{d2}^2 = 1 \qquad (5a)$$

where F_{di} (i = 1,2, for the two respective layers) is the estuarine Froude number:

$$F_{di}^2 = \frac{Q_i^2}{g\frac{\Delta\rho}{\rho_2} l_i^2 H_i^3} = \frac{Q_i^2}{g' l_i^2 H_i^3} = \frac{Q_i^2}{g\beta s_2 l_i^2 H_i^3} \qquad (5b)$$

This formula is valid provided the friction forces and entrainment processes and negligible. Another prerequisite is that the internal Rossby radius, λ, given by eq. (5c) is less than the width (l_i) of the sounds.

$$\lambda = \sqrt{g'H_i/f} \qquad (5c)$$

In eq. (5c) g' is the gravity constant reduced by the factor $\Delta\rho/\rho_2$ and f is the Coriolis parameter. Values typically give $\lambda \approx 1.5$ km, which is of the same order of magnitude as the width of the conjoined ORK sounds. At the mouth of the fjord and in combination with salt and water conservation, Stigebrandt (1975) gives the following relation for the assumed rectangular mouth of the fjord:

$$P^3 \left(1 + \frac{\eta^3}{(1-\eta)^3}\right) - 2P^2 + P = \frac{\eta^3}{F_e^2} \qquad (6)$$

where $P = Q_e/Q_f$ and η is the fraction of the lower layer and the total depth of the fjord mouth. F_e is given by eq. (5b). Skanssund does not have a rectangular section, but is more triangular-shaped. Assuming an exact triangular section, a horizontal line that divides the transect area in two halves is the fraction $(1 - 1/\sqrt{2})$ of the maximum depth below surface. Twice this distance would be an adequate approximation to an equivalent rectangular depth. The corresponding width follows from area equivalence.

In Figure 17 matching P and η numbers of eq. (10) are depicted for various F_e numbers, indicated by corresponding Q_f ratings. The coordinate along these loci that actually will be realized is determined by the wind forcing. Stigebrandt (1975) has developed this theory for fjords with narrow mouths and a sill; these formula are deferred to Appendix II. The numbers indicated in Figure 17 are windspeeds in m/s. The interpretation is therefore that for light winds, high η-values

combine with small P-values. As the wind mixing increases, the p-values also increase until a maximum is reached, generally for $\eta = 0.5$. This P corresponds to the maximum dynamic capacity of the fjord and cannot be exceeded. If the wind mixing is further increased in excess of this value, the well-mixed brackish layer is pushed farther below, but the estuarine flow does not increase. The branch of the curves for $\eta < 0.5$ has thus no physical interpretation. The actual mean wind over a period long enough to permit a steady state to be established (21 days; see eq. (4)), gives a yearly average of 8.96 m/s; see Table 4. A method of calculation using the cubic root of mean sum of the absolute wind measure cubed was adopted from Stigebrandt (1983). These wind speeds are from the Landsort logging. Taking the regression coefficient factor 0.62 (see Section 3.3), one obtains 5.55 m/s for the yearly average in Himmerfjärd.

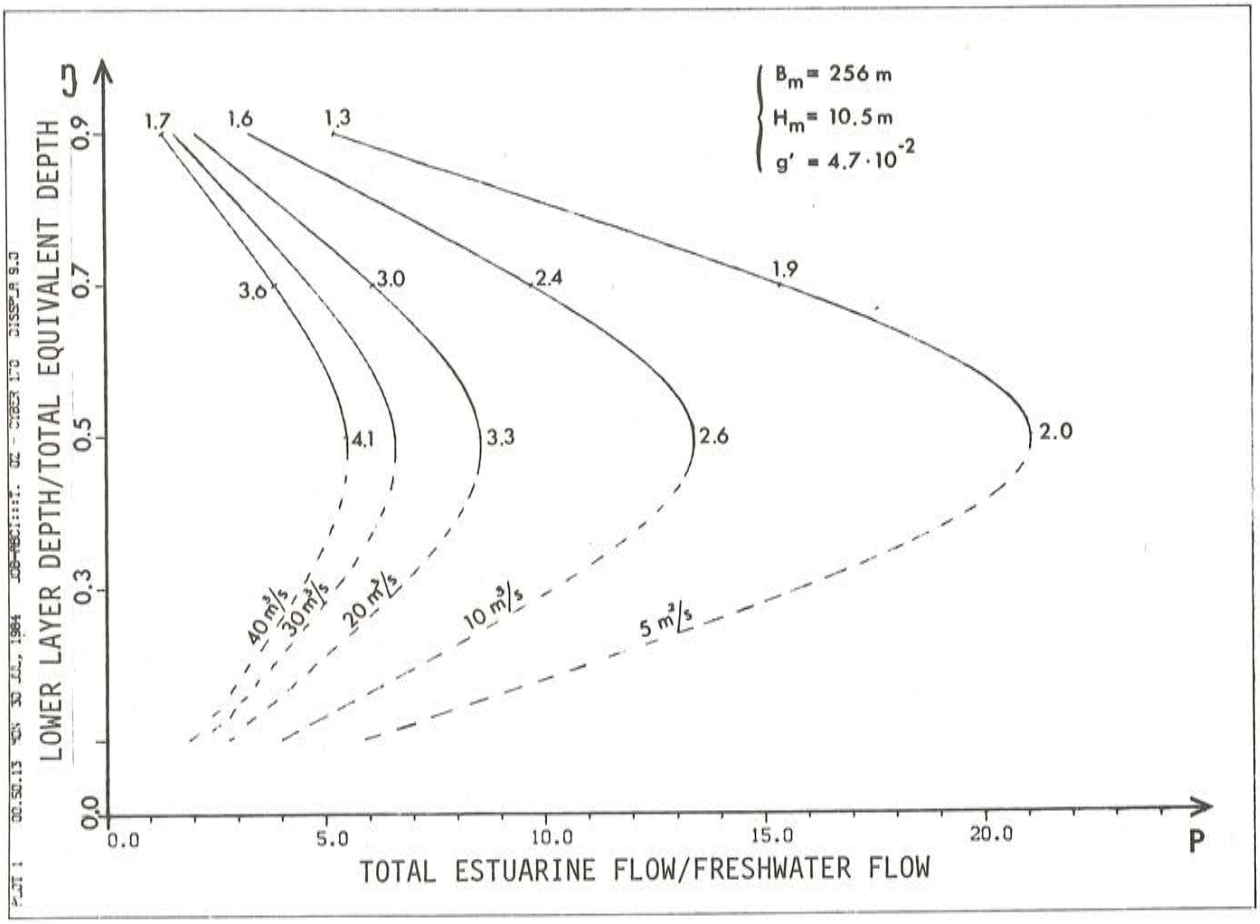

Figure 17. Loci for different freshwater flows in a P/η-diagram over Skanssund with wind as parameter, according to Stigebrandt (1975). The broken lines for $\eta < 0.5$ indicate that these parts lack physical interpretation.

According to this theory, the fjords north of Skanssund are even after the applied correction factor still typically over-mixed. This is called an 0-fjord in Stigebrandt's (1981) classification. The maximal P value for 10 m^3/s is about 13, meaning that an estuarine flow of approximately 130 m^3/s would be expected as typical.

It could, however, be suspected that the estuarine circulation component would be choked, since barotropic flows (those due to sea level slopes) of the same magnitude or larger would for a considerable fraction of a given time period obstruct the barotropic flow in the narrow section. If this is the case, the two-layer transport capacity and thereby the estuarine circulation may increase, (Stigebrandt, 1982). Another argument is that it is questionable that the nondirectional windspeed should be used for these calculations. The fjords are quite narrow and elongated, hence land lee effects can be suspected. It could be possible that a weighted sum of the north-south and east-west component is more realistic. For the conjoined southern sounds ORK it is not likely that this theory applies even if perturbating barotropic flows were not present. The width of the conjoined sections is too large to give a distinct dynamic control regime of the kind discussed above (A. Stigebrandt, pers. comm.), since their conjoined width is greater than the Rossby radius of ca 1.5 km.

8.3 Wind-driven circulation

In order to evaluate the wind-driven flow, half of the transport needed to make up for water level changes is subtracted from the total simulated surface water transport, integrated down to the depth where the reverse flow takes place. This is somewhat incorrect, since the barotropic flow due to water level changes should be evenly distributed over depth. The upper and the lower layers will get equal amounts only if the layers interface at the level that divides the sound area into two halves. For the intended scheme this introduced error is of less importance since it is small in

comparison to the remaining components. The remaining components are the estuarine and the wind-driven flows, Q_e and Q_w, for the two sounds SS and ORK respectively. In Figure 18 scatterplots over the simulated $Q_e + Q_w$ flows vs. the corresponding wind component employed are depicted for ORK and SS respectively. The points corresponding to the high freshwater flushing during simulation period 2b are marked with rings instead of squares. Excluding these rings for a moment, one sees that a rough way of describing these curves is that they have a linear section between two asymptots parallel to the wind axis. This could be interpreted as the physically

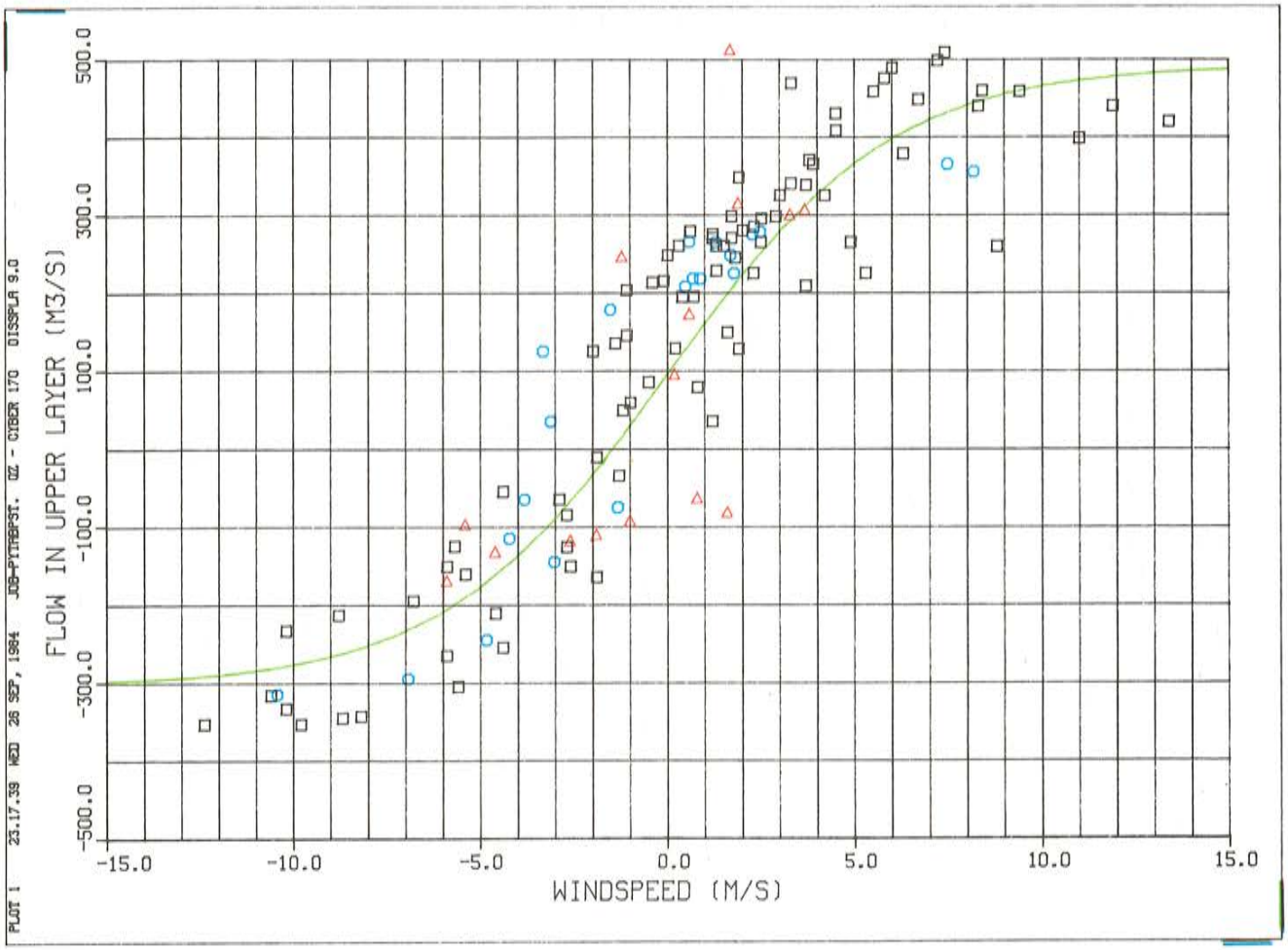

Figure 18 a. Scatter diagram over the ORK sounds with surface flows vs. windspeed. The surface flow has been corrected by subtracting the component due to waterlevel changes as to make the effect of the wind and estuarine flows clearer. The black squares denote corresponding values of daily averages of wind and surface flows (thus defined) for all *simulated* periods except #2b, the spring flood period. This latter is shown with blue rings. A slight but significant increase of the average can be noted for these. For comparison corresponding measurement-based values of the validation period are given by the red triangles. The green curve is the tangent hyperbolicus-fitted function.

plausible mechanism that at windspeeds exceeding a given level, further increase in water transport is limited by the cross-section area throttling the flow. It could also be argued that any wind dependence on the transport would be symmetric in sign. The ultimate argument for this is that the basic hydrodynamic equations are invariant if the horzontal axis is reversed, i.e. if x is substituted for -x. The enhanced scatter of the measured data in Figure 18 is partly due to the systematic absence of observations at high windspeeds.

A simple mathematical function that has these properties of being symmetric and reasonably linear between the asymptots is the tangent hyperbolicus function:

$$\tanh(x) = \frac{e^{x} - e^{-x}}{e^{x} + e^{-x}} \qquad (7)$$

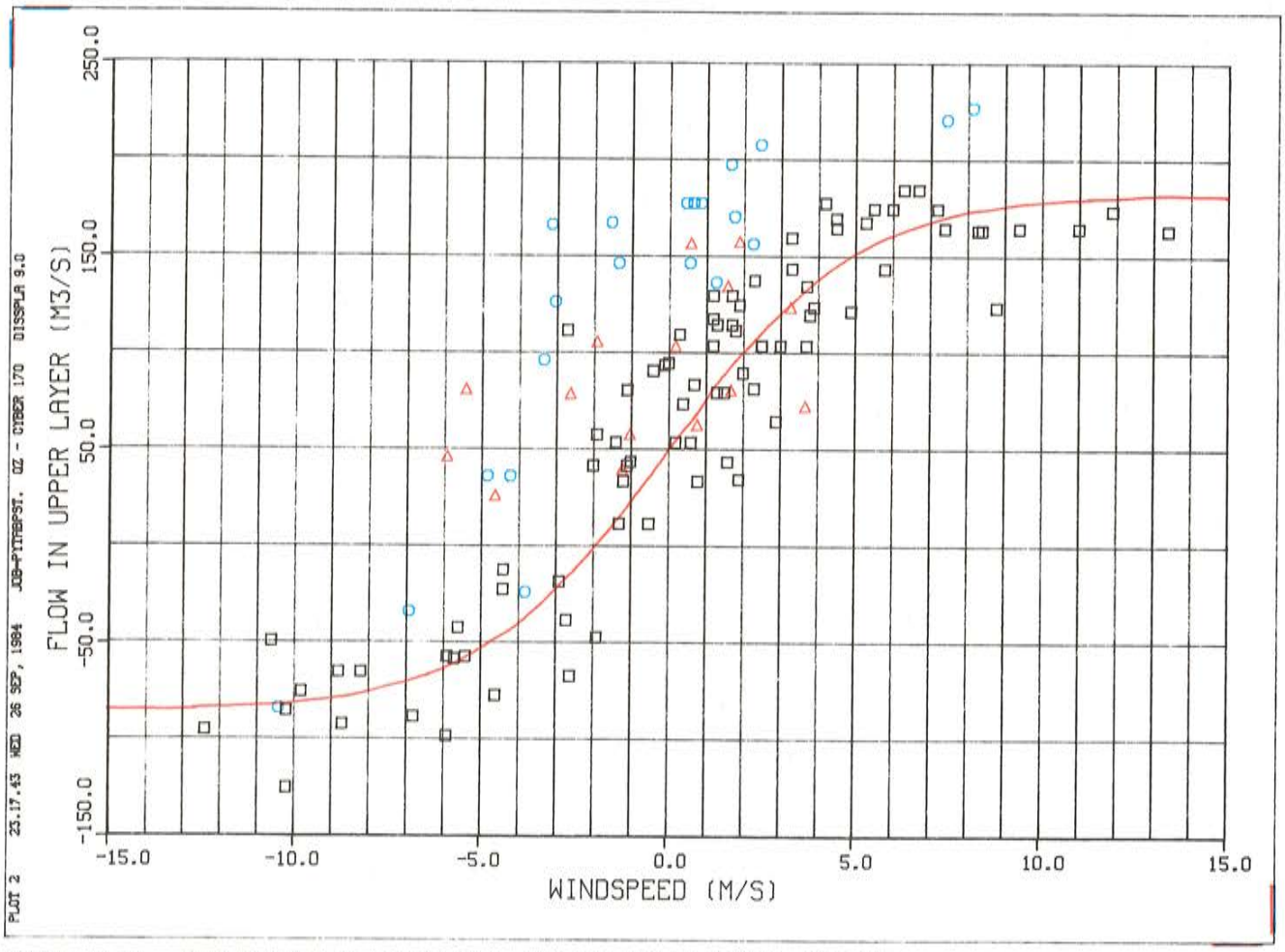

Figure 18 b. Same diagram as Figure 18 b. but for the SS sounds. Here the fitted function is in red.

In Figure 18, a curve of this type, multiplied by a suitable factor of 400 m^3/s for ORK and 135 m^3/s for SS, has been drawn. The wind axis has been scaled so that x is substituted for W/6 and W/5 respectively. This is a pseudo-statistical fit of the data, and serves as a reasonably accurate mathematical shorthand of the relationship between the wind component and the simulated transport.

For windspeeds of 0 m/s these curves give a residual flow of approximately 100 m^3/s and 50 m^3/s for the ORK and the SS sound(s) respectively. This represents the average mean estuarine flow taken over the simulation periods collectively, still excluding period 2b. For this period, however, a significant elevation of the average can be observed. Although the number of points is much less, an estimate of the increased estuarine flow component could be 175 m^3/s and 125 m^3/s respectively. The different estimates are summarized in Table 6.

From this table it is clear that there exists an interesting and challenging discrepancy between the different estimates. The most disconcerting property of the model is the output for the ice-cover period. Not only is the residual vertical eddy-diffusivity much too high considering that the wind forcing is zero, but also the transport in SS is higher compared to the ice-free period. The only way to explain this is to evoke the choking hypothesis again. It is reassuring, though, that Rydberg (1981) found that for a certain fjord (Byfjord) at a constant freshwater forcing, the estuarine flow could vary by a factor of 4, depending on which regime (3-layer, 2-layer O-fjord or 2-layer N-fjord) would be established.

The scatter of the points around this tangent hyperbolicus function depends mainly on the inertial and densometric forces completely neglected here. Of course a full battery of statistical regression analyses could be undertaken. However this seems beside the point, since the purpose is not to arrive at an accurate best-fit estimate of a one-day time resolution, but to assess the water turnover on an intermediate time scale

longer than one day. Figure 19 gives the spectral behavior of the wind the last 256 days in 1977, thus excluding the ice-cover period. From this spectrum it is clear that the two peaks for the time periods (=inverse of frequency) of 5 days and 3 days means that the wind surges on the average persist during at least half of these periods. If the average thus is established on a basis of about 3 days instead of one (as is done in Figure 15), the scatter would consequently be considerably diminished. The lack of a distinct peak for a time period of one day means that the diurnal wind fluctuation from the land- and seabreeze effect is filtered off, since this would be mainly acting on the east-west component that is discarded in the forcing of the model.

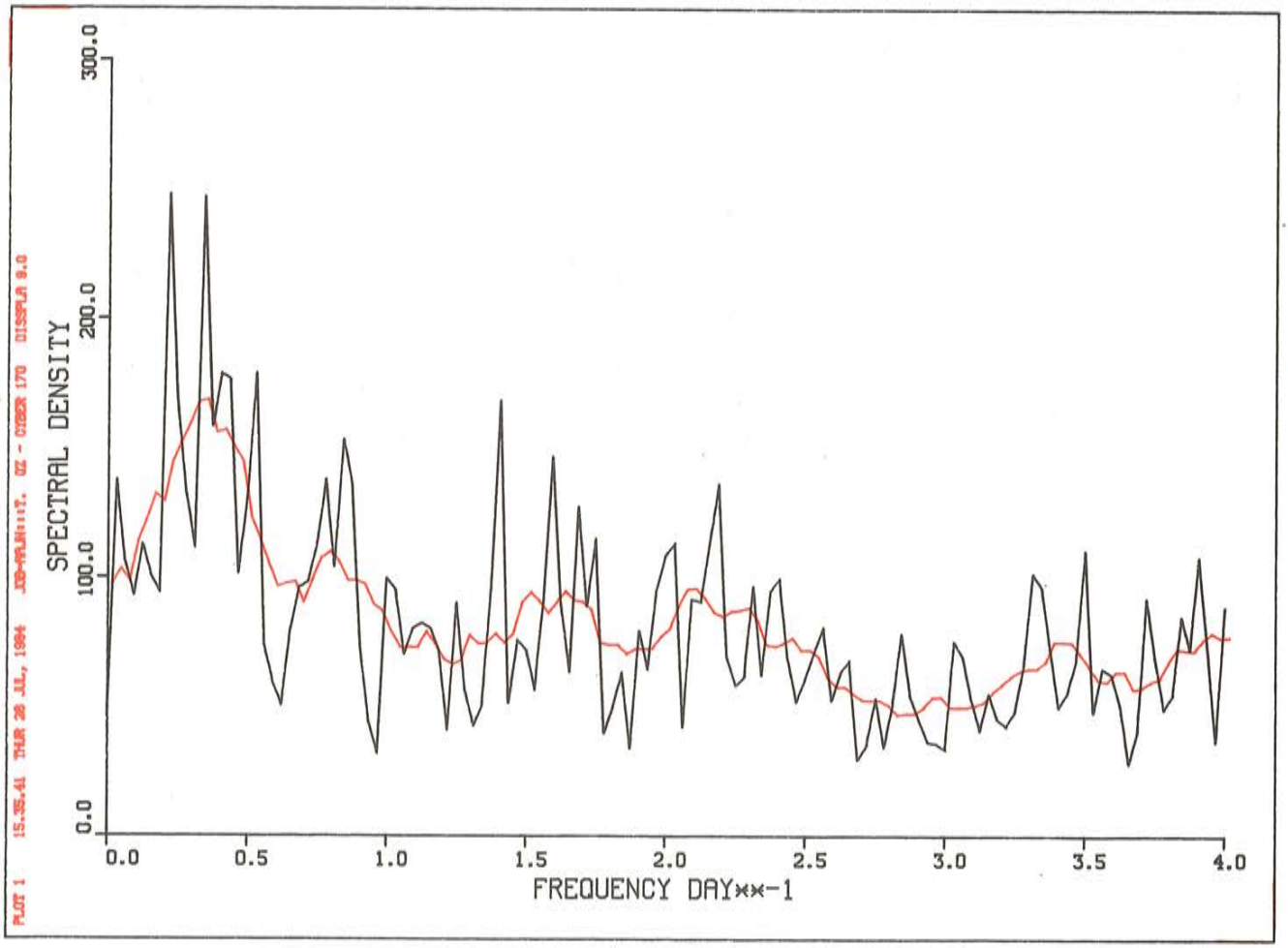

Figure 19. Spectrum of the wind N/S-component at Landsort for the last 256 days of 1977, thus excluding the ice period. The Nyqvist frequency is 4 day^{-1}, meaning that 8 observations per day were processed. Two distinct peaks for 5- and 3-days period time can be noted at the low frequency part of the curve. A running average is shown in red, to make the general trend more conspicuous, namely that the wind energy is dominated by low-frequency surges.

8.4 Whole-year estimate

To sum up the findings and arguments in the previous sections, a "hypermodel" of the circulation model can be formulated now:

ORK

$$Q_w(W) = 400 \cdot \tanh(W/6) \quad [m^3/s] \quad (8)$$

$$Q_e(t) = 0.9 \cdot Q_e(t-1) + 0.1 \cdot (2.5\, Q_f + 75) \quad [m^3/s] \quad (9)$$

SS

$$Q_w(W) = 135 \cdot \tanh(W/5) \quad [m^3/s] \quad (10)$$

$$Q_e(t) = 0.9 \cdot Q_e(t-1) + 0.1 \cdot (2.5\, Q_f + 25) \quad [m^3/s] \quad (11)$$

For Q_{wl} the piece-linear approximation is used; see Table 3. This refers to the ORK sounds. For the SS sound the value used is smaller in proportion to how the surfaces compare north and south of Skanssund. The formulae for the estuarine flow, eqs. (9) and (11), are based on the model's output linearly interpolated for freshwater flows between 10 and 40 m^3/s. To smooth the transition from changes in the Q_f input, an AR-process mechanism has been employed to give a timescale for changes according to eq. (4).

For the ice-cover period the circulation model output is unrealistic and therefore is discarded. Instead, the more realistic P values 3 for ORK and 2 for SS are chosen, consistent with the equations in Appendix II. The result of this attempt can be seen in Table 5 where days of continuity in the sign of the wind component are grouped together and averaged.

Again the same Q_{wl} component is added to the upper layer of the hypermodel estimates Q_{tot}, in order to make it comparable to Q_{sim} from which it was subtracted when estimating Q_w and Q_e.

A three-day running average proposed by the spectral considerations in the previous section of the summed components is shown in Figure 20a and b. As could be expected, the fit

between the simulated surface layer flows in SS and ORK (red and green curve in Figure 20a and b respectively) and the corresponding hypermodel estimates (blue curve) is much better than the scatter in Figure 18 would lead one to believe; the curves represent the first coarse but approximately correct whole-year estimate for Himmerfjärd. Since the statistical part of the approach has been restricted to a simple one-factor regression, the curves shown could be regarded as typical of the method, leaving room for further improvement.

In the first place, it seems more appropriate to achieve better estimates by improving the circulation model's physical foundation in accordance with e.g. Stigebrandt's

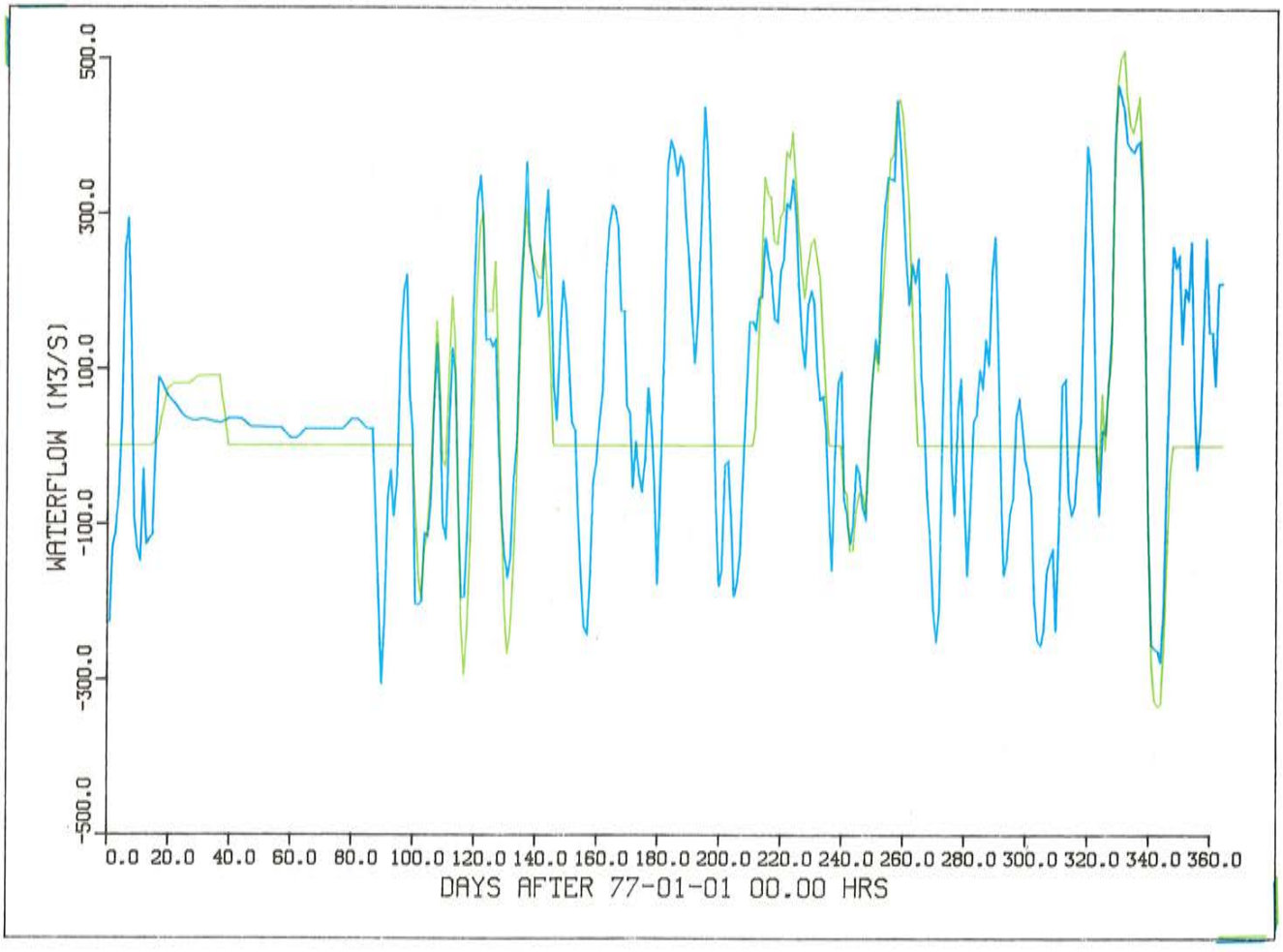

Figure 20 a. A comparison between the *simulated* curve of Figure 15 (green) and the "hypermodel" computation (blue) of the surface flows in the ORK sounds for the entirety of 1977. The latter curve is computed on daily basis, but both curves are filtered by a 3-day running averaging process. The gaps between the simulated periods are set to zero. This in combination with the filtering process makes the edges less sharp compared to the corresponding curve in Figure 15.

parametrization; afterwards eqs. (8)-(11) could be revised. The ice-cover period in particular calls for better understanding. The daily mean flows in either direction over a one-year average given below the broken bottom line in Table 5 allow a possibility (suggested by A. Stigebrandt) of checking the long-time validity of the model. For every 10 m^3 freshwater flowing in through SS, there will on the average be 49+26-34 = 41 m^3 brackish water flowing out, meaning an effective P-value of 4.1. If the salinity of representative bottom water flowing in during one year were about S_b = 6.4 o/oo (see Figure 9a), the averaged salinity of the outflowing surface water would be 3.1 • 6.4/4.1 = 4.8 o/oo (=S_s). Regrettably there were no salinity samples taken north of SS during 1977. The sole instance when a complete salinity profile was sampled took place 77-09-13 at a

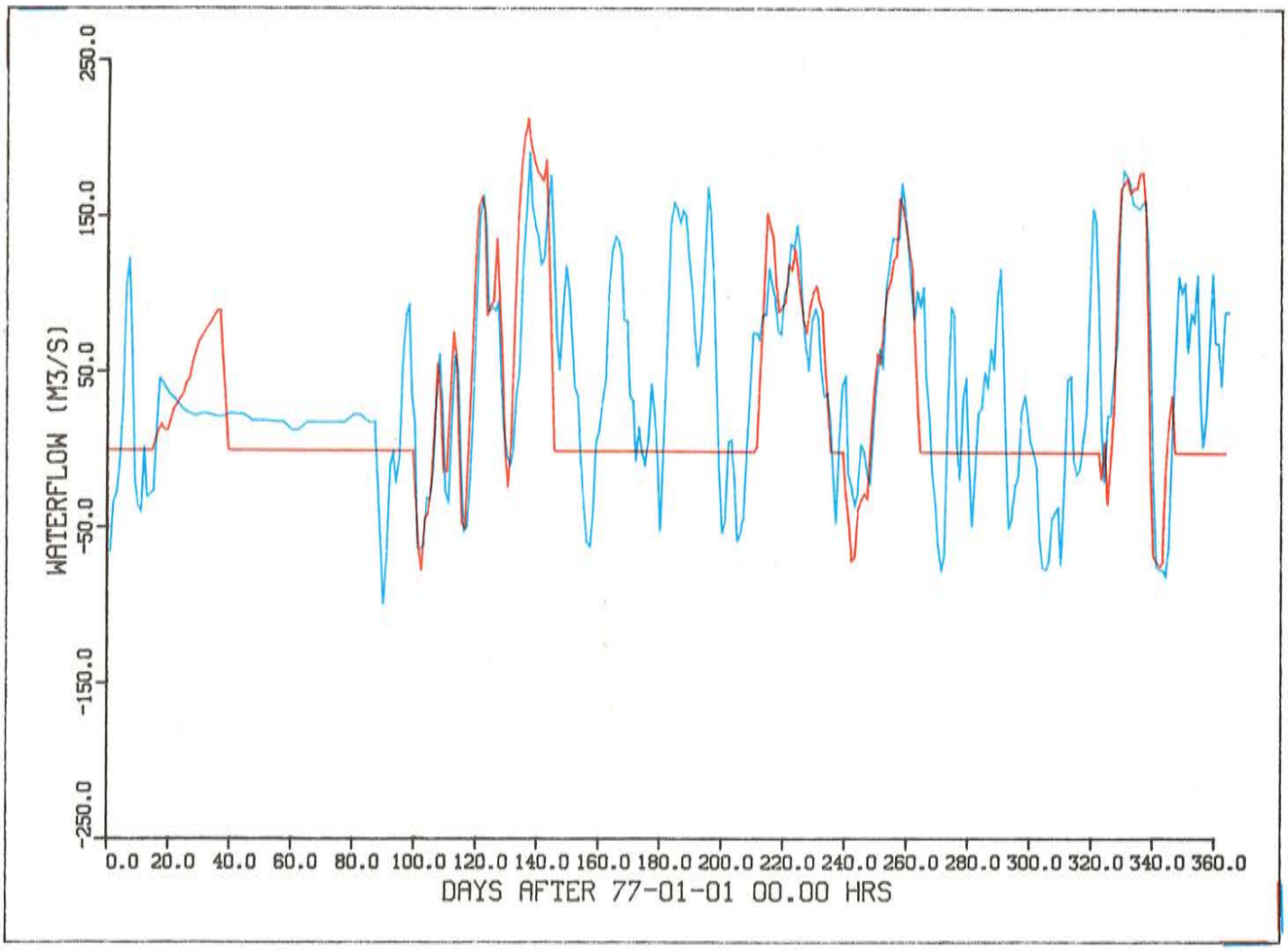

Figure 20 b. Corresponding curves to Figure 20 a, but for the SS sound. The simulated curve is shown in red and the hypermodelled in blue. Except for the ice period, the fit is convincing, though the hypermodel tends to underestimate systematically.

station somewhat south of SS. With the observed averaged values S_b = 6.4 o/oo and S_s = 5.5, eq. (12) gives a P-value of 7.1.

$$P = \frac{S_b}{S_b - S_s} \qquad (12)$$

Now the salinities in eq. (12), which follows directly by the definition of the P-factor and salt conservation, are supposed to represent typical water flowing in and out, unaffected by the vertical diffusive exchange that necessarily takes place in a narrow sound. Therefore no conclusion can be based on this unique observation.

The high degree of explanation ($\bar{r}^2_{ork}$ = 86 % and $\bar{r}^2_{ss}$ = 78 % according to Table 7) still apparent between the circulation model and its hypermodel (disregarding the ice-cover period) reveals a simple overall relationship between wind forcing and water transport through the sounds. In retrospect it is not surprising that the circulation model works this way, since the wind-stress affects the upper-layer vorticity and is then diffused downwards. The question is how real estuaries function.

Many various theories can be found in the literature concerning wind forcing and current speed at different depths (cf. Svensson, T., 1980) but these formulae are quite difficult to integrate in time and depth to obtain the water transport. Therefore it is not plausible that future estimates can be attained in the complete absence of modelling.

9. CONCLUSIONS

The circulation model regenerates the flow pattern (i.e. current as a function of time and depth) in the two sounds SS and ORK for the validation period. This is done so convincingly that it no doubt mimics the dominating mechanisms that are responsible for the water turnover. This would not be surprising if calibrational manipulation with the model had been the case, but no tuning was undertaken for the validations

phase. The parameters were chosen prior to the simulations. This fact strongly corroborates the model.

In addition, the model with this initial set of parameters turned out to produce depth-integrated surface layer transports that were coherent with measurement-based computed data. Since the latter data are sampled daily and the former are available as model output 24 times more frequently (i.e. hourly), it is reassuring if not convincing to note that measured data with virtually no exception fall within the fluctuations around the running average of simulated data, making allowances for the exact time of day the samples were taken. This scatter is mainly caused by the 4-hour seiche and the wind spectrum components with shorter time periods than one day.

Of the four different forcings, the one due to changes in the water-level is most convincing, both in the way it has been sampled (two independent observations coincide almost completely) and the modelling of its mechanisms. The 4-hour seiche is found to give no or negligible contribution by its direct action, but it is uncertain to what extent it influences the circulation by other means, e.g. tidal choking and increased mixing in the sounds. The wind-driven flows are modelled by the windstress influence on the vorticity field.

It is found that, complex as this mechanism may appear, a simple mathematical function with the N/S-component of the wind as independent variable regenerates daily transports so well that the degree of explanation (r^2) is about 80 %. This is valid for the total surface flows which also contain the estuarine flow component. The latter is normally much smaller than the former. Since wind influence was null for a three-month ice period in 1977, their yearly averages one comparable. The estuarine flows simulated by the model are more doubtful and are a consequence of too high vertical mixing parameters. These could not be chosen freely in this study because of economical reasons in the first place and numerical reasons in the second.

One can be quite confident about the model's capacity to deal with the seasonal variation of the S&T fields since the physical processes involved are well represented. The only calibration of the model was when checking the parameter revision prior to the seasonal runs did not make the simulated transport estimates of the validation period inferior in comparison to the initial ones. It is therefore plausible that the model simulations are valid for the other chosen seasons distributed over the year.

The fact that a large part of the variation in the model transport output put can be explained by a relatively simple "hypermodel" implies if the resulting lowered temporal resolution can be accepted that a detailed description of the oceanography may not be called for. The seasonal variation of the density field, for example, seems to only marginally affect the wind-driven flow component. On the other hand, its influence on the estuarine flow may be substantial. To discriminate between this and other model implications, there is an urgent need for more field data, preferably amassed as to provide the most accurate transport estimates possible. In particular, this means in the light of the present study, temporally equidistant and more frequent data. Based on only the transport estimates the model could possibly have a relative error as much as ± 50 %. A more conservative estimate also considering the flow pattern comparisons would reduce this estimated error by a factor two.

If this inaccuracy level can be accepted, e.g. for material budgeting, the present method can be used without any modifications. It must here be pointed out that the relative error - be what it may - with almost complete certainty is systematic. This means that comparative studies based on the model estimates still can be conclusive in spite of the large relative error the compared items share. In other words: A model's precision may be better than its accuracy.

To improve the present results there are a host of different ways to proceed, all with their respective advantages and disadvantages. The most attractive ones are to run whole-year simulations on a supercomputer or refine the hypermodel approach so that yet more of the variation (that here is not accounted for, i.e. scatter) could be included as mechanism.

This is not, however, the place to discuss the pros and cons of future Himmerfjärd circulation models at any length. Instead it can be concluded that the model approach per se has been successful and that a first coarse, but approximately correct, whole-year estimate for the water turnover in Himmerfjärd now has been achieved, which was the main objective of this study.

Table 0. Thanks to those who thanks deserve.

	Affiliation	Financial support	Inspiration	Discussion	Proofreading	Typing	Drafting	Printing	Computer assistance	Data acquisition	Deep gratitude	Thanks
QZ (Stockholm Univ. Computer Dept.)								×				×
SMHI (Swed. Meteorol. & Hydrol. Inst.)					×		×	×		×		×
SNV (Swed. Natl. Board of Envir. Prot.)		×								×		×
Lars Andersson	Ferryboat, Skanssund								×			×
Erland Bergstrand	SMHI		×									×
Ragnar Elmgren	ZISU	×	×									×
Ida Engqvist	A.Engqvist			×		×				×		×
Mats Hamrud	MISU							×				×
Olle Häggroth	Pilot, Södertälje								×			×
Björn Kjerfve	Univ. of South Carolina		×	×						×		×
Ulf Larsson	ZISU	×		×					×			×
Leif Lundgren	Askölab.								×			×
Lars Rydberg	OIGU			×								×
Bernt Samuelsson	SMHI							×				×
Anders Stigebrandt	OIGU		×	×						×		×
Rolf Söderlund	MISU								×			×
Greta Ågren	ZISU	×										×

MISU = Meteorol. Inst., Stockholms Univ.
OIGU = Oceanographical Inst., Gothenburg Univ.
ZISU = Zoological Inst., Stockholm Univ.

Table 1. Comparison of estimated and modelled hypsographical parameters. The uncertainty is greatest for the estimation of sound areas. Some other parameters pertaining to the respective categories are included.

Location	Average Length (km)	Width (km)	$10^6 m^2$	Estimated $10^6 m^2$	Modelled $10^6 m^2$
Surface Areas:					
Näslandsfjärd	10	1.3	13.5		
Hallsfjärd	10	0.6	6.4	26.6	27.0
Stafsbofjärd	10	0.7	6.7		
Kaggfjärd N	4	1.3	5.3	8.1	8.0
Kaggfjärd S	3	1.0	2.8		
Himmerfjärd inner basin	10	2.8	28.0	28.0	29.5
Total				62.7	64.5

Location	Average Depth (m)	$10^6 m^3$	Estimated $10^6 m^3$	Modelled $10^6 m^3$
Volumes:				
Näslandsfjärd	13	175.0		
Hallsfjärd	17	108.0	336.6	337
Stafsbofjärd	8	53.6		
Kaggfjärd N	12	63.6	106.6	108
Kaggfjärd S	15	42.0		
Himmerfjärd inner basin	18	504.0	504.0	508
Total	15		946.2	953

Location	Minimum Width (km)	Average Depth (m)	Maximum Depth (m)	Estimated $10^3 m^2$	Modelled $10^3 m^2$
Sound Areas:					
Skanssund	0.30	8.5	18	3.2	3.2
Oaxen-Regarn	0.45	11.0	16		
Regarn-Koholm	0.35	5.2	8	7.8	9.1
Mörkö-Oaxen	0.65	2.7	7		
Uddsund	0.25	20.0	23	5.0	-
Kaggfjärd N/S	0.25	4.8	12	1.2	-
Pålsund	0.15	2.6	5	0.4	-

Table 2. Overview of model parameters. For the validation run the Svensson and Wilmot (1978) set was used with no alterations.

			Wilmot (1976)	Svensson & Wilmot (1978)	Jørgenssen (1979)	Buch (1980)	Present model (1984)
Area of application			Bråviken	The Sound	various	Hf jd	Hf jd
Horizontal eddy diffusivity	K_H	(cm^2/s)	$5 \cdot 10^6$	$1 \cdot 10^5$	$56-1.4 \cdot 10^6$	$2 \cdot 10^3$[a]	$5 \cdot 10^4$
Horizontal eddy viscosity	A_H	(cm^2/s)	$5 \cdot 10^6$	$5 \cdot 10^4$			$5 \cdot 10^4$
Vertical eddy diffusivity	K_V	(cm^2/s)	5	40	10^{-2} -2	$2 \cdot 10^{-2}$	20[c]
Vertical eddy viscosity	A_V	(cm^2/s)	5	40			20
Molecular salt diffusion		(cm^2/s)		$1 \cdot 10^{-5}$	$2 \cdot 10^{-6}-6.2 \cdot 10^{-5}$		$1 \cdot 10^{-5}$
Molecular heat diffusion		(cm^2/s)		$1.5 \cdot 10^{-3}$	$1.6 \cdot 10^{-3}$		$1.5 \cdot 10^{-3}$
Molecular viscosity		(cm^2/s)		$1.35 \cdot 10^{-2}$			$1.35 \cdot 10^{-2}$
Diffusion lower layer factor		--		0.8	$10^{-2}-100$[b]		0.8
Wind stress factor		(cm^2/s^2)		6.4			6.4
Wind mixing vorticity		(cm^2/s^3)		$4 \cdot 10^{-2}$			$4 \cdot 10^{-2}$

[a] pycnocline

[b] thermocline

[c] 50 cm^2/s during initial 24 h

Table 3. Flows determined by changes of water level at Södertälje locks. Positive values of Q_{wl} means filling.

Period (Julian days)	Number of Days	Water Level (cm)	Q_{wl} (m^3/s)
0- 5	6	-9	-10
6- 10	5	10	25
11- 18	8	-15	-20
19- 23	5	-15	0
24- 29	6	0	16
30- 38	9	0	0
39- 45	7	-19	-18
46- 58	13	-19	0
59- 63	5	0	25
64- 78	15	0	0
79- 83	5	-19	-25
84- 88	5	-19	0
89-101	13	1	10
102-114	13	21	10
115-129	15	-2	-10
130-136	7	-13	-10
137-142	6	-18	-5
143-159	17	8	10
160-166	7	-4	-12
167-176	10	-4	0
177-180	4	20	40
181-192	12	9	-6
193-196	4	29	32
197-208	12	29	0
209-212	4	19	-16
213-222	10	19	0
223-232	10	-27	-30
233-240	8	-20	6
241-260	20	35	18
261-265	5	16	-25
266-270	5	-7	-30
271-274	4	21	45
275-294	20	-10	-10
295-324	30	64	16
325-344	20	-13	-25
345-364	20	12	8
	365		

Table 4. Calculation of the average wind over the year. Cubic root of mean sum of cubes method $\overline{W} = \sqrt[3]{\sum_{n=1}^{N} \frac{W^3}{N}}$ has been employed. Bases are SMHI 3-h windlogging at Landsort.

Day Number	$\overline{W}$	Day Number	$\overline{W}$
0- 20	9.3	180-200	8.8
20- 40	8.8	200-220	7.0
40- 60	8.1	220-240	6.2
60- 80	8.4	240-260	10.6
80-100	9.3	260-280	10.1
100-120	8.1	280-300	8.3
120-140	8.8	300-320	11.4
140-160	6.8	320-340	9.7
160-180	7.2	340-360	10.6

Table 5. Synopsis of simulated (SIM) and hypermodelled (QTOT) flows in the upper layers of ORK and SS. Because of opposite sign convention, Q_{wl} is reversed compared to Table 3. The two bottom lines denote the sum of the pos. and neg. daily components respectively, divided by 365. This yields thus the yearly average of each component.

					ORK					SS				
	INTERVAL	DAYS	W(N/S)	QF	SIM	QTOT =	QWL/2 +	QE +	QW	SIM	QTOT =	QWL/2 +	QE +	QW
	0- 5	6	-5.9	10.0	0.	-137.	5.	100.	-242.	0.	-36.	2.	50.	-88.
	6- 8	3	4.5	10.0	0.	302.	-13.	100.	214.	0.	124.	-5.	50.	79.
	9- 12	4	-4.9	10.0	0.	-142.	-2.	100.	-241.	0.	-40.	-1.	50.	-89.
	13- 16	4	-5.1	10.0	0.	-57.	10.	98.	-165.	0.	-7.	4.	49.	-60.
#1	17- 18	2	-.1	10.0	20.	94.	10.	84.	0.	20.	47.	4.	43.	0.
#1	19- 23	5	.0	10.0	76.	67.	0.	67.	0.	20.	36.	0.	36.	0.
#1	24- 29	6	-3.6	10.0	82.	43.	-8.	51.	0.	47.	26.	-4.	29.	0.
#1	30- 38	9	-1.2	10.0	90.	40.	0.	40.	0.	82.	24.	0.	24.	0.
	39- 45	7	2.0	10.0	0.	43.	9.	34.	0.	0.	25.	4.	22.	0.
	46- 58	13	2.6	10.0	0.	32.	0.	32.	0.	0.	21.	0.	21.	0.
	59- 63	5	.3	10.0	0.	18.	-13.	31.	0.	0.	15.	-5.	20.	0.
	64- 78	15	-2.3	10.0	0.	30.	0.	30.	0.	0.	20.	0.	20.	0.
	79- 83	5	-.1	10.0	0.	43.	13.	30.	0.	0.	25.	5.	20.	0.
	84- 88	5	2.7	10.0	0.	30.	0.	30.	0.	0.	20.	0.	20.	0.
	89- 93	5	-4.6	10.0	0.	-146.	-5.	48.	-190.	0.	-42.	-2.	28.	-68.
	94- 95	2	-5.5	10.0	0.	-228.	-5.	65.	-288.	0.	-75.	-2.	35.	-108.
	96- 99	4	3.8	10.0	0.	259.	-5.	74.	190.	0.	107.	-2.	39.	71.
	100-101	2	-4.3	10.0	0.	-162.	-5.	81.	-238.	0.	-50.	-2.	42.	-91.
	102-105	4	-4.5	10.0	-158.	-144.	-5.	86.	-226.	-55.	-42.	-2.	44.	-84.
#2	106-108	3	-.8	10.0	47.	56.	-5.	90.	-30.	13.	34.	-2.	46.	-10.
#2	109-112	4	-2.9	10.0	15.	-81.	-5.	93.	-170.	0.	-20.	-2.	47.	-65.
#2	113-114	2	2.1	10.0	230.	222.	-5.	95.	132.	95.	99.	-2.	48.	53.
#2	115-119	5	-5.0	30.0	-220.	-140.	5.	110.	-255.	-20.	-31.	2.	62.	-95.
#2	120-122	3	3.6	30.0	200.	330.	5.	124.	201.	157.	154.	2.	75.	77.
#2	123-127	5	.5	40.0	218.	183.	5.	139.	39.	114.	108.	2.	90.	16.
#2	128-131	4	-5.7	40.0	-123.	-113.	5.	153.	-271.	25.	5.	2.	104.	-101.
#2	132-136	5	-1.2	40.0	-10.	79.	5.	161.	-87.	130.	79.	2.	111.	-35.
#2	137-141	5	1.3	40.0	246.	251.	3.	167.	81.	190.	151.	1.	117.	32.
#2	142-145	4	2.3	25.0	198.	272.	-3.	165.	111.	140.	154.	-1.	115.	41.
	146-148	3	-1.6	10.0	0.	41.	-5.	146.	-101.	0.	54.	-2.	96.	-40.
	149-150	2	2.4	10.0	0.	278.	-5.	135.	147.	0.	142.	-2.	85.	58.
	151-154	4	-1.6	10.0	0.	20.	-5.	126.	-101.	0.	34.	-2.	76.	-40.
	155-159	5	-6.6	10.0	0.	-190.	-5.	116.	-300.	0.	-45.	-2.	66.	-109.
	160-162	3	-1.4	10.0	0.	40.	6.	110.	-76.	0.	34.	3.	60.	-29.
	163-166	4	3.3	10.0	0.	310.	6.	107.	197.	0.	137.	3.	57.	77.
	167-171	5	.4	10.0	0.	136.	0.	105.	31.	0.	67.	0.	55.	13.
	172-176	5	-2.1	10.0	0.	-30.	0.	103.	-133.	0.	0.	0.	53.	-52.
	177-180	4	-1.5	10.0	0.	12.	-20.	102.	-70.	0.	18.	-9.	52.	-26.
	181-184	4	2.2	10.0	0.	215.	3.	101.	111.	0.	94.	1.	51.	41.
	185-188	4	4.9	10.0	0.	371.	3.	101.	268.	0.	153.	1.	51.	101.
	189-192	4	1.8	10.0	0.	214.	3.	100.	110.	0.	95.	1.	50.	43.
	193-198	6	4.8	10.0	0.	281.	-11.	100.	192.	0.	114.	-5.	50.	68.
	199-203	5	-3.3	10.0	0.	-68.	0.	100.	-168.	0.	-12.	0.	50.	-62.
	204-208	5	-4.9	10.0	0.	-164.	0.	100.	-264.	0.	-49.	0.	50.	-99.
	209-212	4	1.0	10.0	0.	173.	8.	100.	65.	0.	80.	4.	50.	26.
	213-217	5	2.2	10.0	276.	233.	0.	100.	133.	120.	102.	0.	50.	52.
#3	218-222	5	1.8	10.0	286.	211.	0.	100.	111.	96.	94.	0.	50.	44.
#3	223-227	5	2.8	10.0	334.	271.	15.	100.	156.	112.	115.	6.	50.	59.
#3	228-232	5	.9	10.0	244.	176.	15.	100.	61.	98.	80.	6.	50.	24.
#3	233-235	3	-.4	10.0	137.	73.	-3.	100.	-24.	57.	39.	-1.	50.	-10.
	236-240	5	-2.3	10.0	0.	-17.	-3.	100.	-114.	0.	6.	-1.	50.	-43.
#0	241-245	5	-3.2	10.0	-114.	-98.	-9.	100.	-189.	-56.	-27.	-4.	50.	-73.
#0	246-248	3	-3.2	10.0	-63.	-71.	-9.	100.	-162.	-27.	-13.	-4.	50.	-59.
#0	249-253	5	.5	10.0	96.	119.	-9.	100.	28.	50.	57.	-4.	50.	10.
#0	254-256	3	7.6	10.0	310.	355.	-9.	100.	264.	110.	139.	-4.	50.	92.
#0	257-260	4	8.0	10.0	443.	414.	-9.	100.	323.	158.	162.	-4.	50.	116.
#0	261-265	5	1.9	10.0	186.	223.	13.	100.	110.	70.	97.	5.	50.	42.
	266-270	5	-3.1	10.0	0.	-41.	15.	100.	-156.	0.	-2.	6.	50.	-58.
	271-273	3	-5.9	10.0	0.	-203.	-23.	100.	-280.	0.	-63.	-10.	50.	-103.
	274-274	1	10.6	10.0	0.	455.	-23.	100.	377.	0.	172.	-10.	50.	131.
	275-277	3	-2.8	10.0	0.	-19.	5.	100.	-124.	0.	8.	2.	50.	-44.
	278-279	2	1.6	10.0	0.	205.	5.	100.	100.	0.	92.	2.	50.	40.
	280-283	4	-3.9	10.0	0.	-86.	5.	100.	-191.	0.	-19.	2.	50.	-71.
	284-287	4	-.3	10.0	0.	84.	5.	100.	-21.	0.	44.	2.	50.	-9.
	288-291	4	2.2	10.0	0.	237.	5.	100.	132.	0.	103.	2.	50.	51.
	292-294	3	-4.8	10.0	0.	-160.	5.	100.	-265.	0.	-48.	2.	50.	-100.
	295-297	3	-2.4	10.0	0.	-57.	-8.	100.	-149.	0.	-13.	-4.	50.	-59.
	298-301	4	-.9	10.0	0.	48.	-8.	100.	-44.	0.	30.	-4.	50.	-16.
	302-306	5	-7.8	10.0	0.	-205.	-8.	100.	-297.	0.	-59.	-4.	50.	-106.
	307-311	5	-5.6	10.0	0.	-172.	-8.	100.	-264.	0.	-50.	-4.	50.	-96.
	312-313	2	2.9	10.0	0.	263.	-8.	100.	171.	0.	113.	-4.	50.	66.
	314-318	5	-4.4	10.0	0.	-108.	-8.	100.	-200.	0.	-26.	-4.	50.	-72.
	319-322	4	5.6	10.0	0.	378.	-8.	100.	286.	0.	153.	-4.	50.	107.
	323-327	5	-3.6	10.0	-4.	-43.	5.	100.	-147.	-20.	-1.	1.	50.	-53.
#4	328-331	4	7.4	10.0	385.	414.	13.	100.	302.	138.	163.	5.	50.	108.
#4	332-335	4	5.8	10.0	438.	405.	13.	100.	293.	173.	164.	5.	50.	109.
#4	336-339	4	4.5	10.0	398.	351.	13.	100.	238.	165.	144.	5.	50.	89.
#4	340-344	5	-9.9	10.0	-306.	-256.	13.	100.	-369.	-72.	-74.	5.	50.	-129.
#4	345-346	2	-6.7	10.0	-225.	-177.	-4.	100.	-273.	30.	-51.	-2.	50.	-99.
	347-351	5	2.4	10.0	0.	242.	-4.	100.	146.	0.	105.	-2.	50.	57.
	352-355	4	2.1	10.0	0.	207.	-4.	100.	111.	0.	90.	-2.	50.	42.
	356-357	2	-4.7	10.0	0.	-155.	-4.	100.	-251.	0.	-47.	-2.	50.	-95.
	358-360	3	3.4	10.0	0.	277.	-4.	100.	181.	0.	117.	-2.	50.	68.
	361-364	4	2.1	10.0	0.	177.	-4.	100.	81.	0.	77.	-2.	50.	28.
			1.8	12.2	62.	122.	3.	91.	68.	30.	56.	1.	49.	26.
			-2.3	.0	-18.	-52.	-3.	0.	-90.	-5.	-15.	-1.	0.	-34.

Ice period

Table 6. Comparison of different estimations of the estuarine flow, Q_e.

Source	Time Period	Q_f = 10 m^3/s		Q_f = 40 m^3/s	
		ORK	SS	ORK	SS
Toll (1980)	3 months	70	50	-	-
Model:					
Ice-free period	9 weeks	100	50	175	125
Ice-cover period	3 weeks	90	90		
Stigebrandt (1975)	3 weeks	-	130	-	200

Table 7. Correlation coefficients (r) between the simulated and the hypermodel estimated upper layer flows, calculated for the various seasonal periods.

Season no.	r_{ork}		r_{ss}	
1	-0.889		-0.819	
2a	0.901	$\bar{r}_{ork}$ = 92.2%	0.970	$\bar{r}_{ss}$ = 88.2%
2b	0.920		0.858	
3	0.886		0.701	
0	0.920		0.948	
4	0.984		0.985	

APPENDIX I

General hydrodynamic equations (Landau and Lifshitz, 1959):

$$\nabla \cdot \bar{v} = - \frac{1}{\rho} \frac{\partial \rho}{\partial t} \quad ; \qquad \text{Continuity eq.} \qquad (A1)$$

$$\frac{\partial \bar{v}}{\partial t} = - \frac{1}{\rho} \nabla p - (\bar{v} \cdot \nabla) \bar{v} + \mu \Delta \bar{v} - g\hat{z} \quad ; \qquad \text{Momentum eq.} \qquad (A2)$$

$$\frac{\partial T}{\partial t} = - \bar{v} \cdot \nabla T + \frac{1}{\rho c_p} \left[\nabla \cdot \kappa \nabla T + \sigma'_{ik} \frac{\partial v_i}{\partial x_i} \right] ; \qquad \text{Heat eq.} \qquad (A3a)$$

$$\frac{\partial S}{\partial t} = - \nabla \cdot (\bar{v} S) + \nabla \cdot (\bar{K}^S S) + k \Delta S \quad ; \qquad \text{Salt eq.} \qquad (A3b)$$

$$\rho = \rho(p,T,S) \quad ; \qquad \text{State eq.} \qquad (A4)$$

Time-averaged model equations, according to Bork (1978):

$$\frac{\partial u}{\partial x} + \frac{\partial w}{\partial z} = 0 \ , \ (v \equiv 0) \quad ; \qquad (A5)$$

$$\frac{du}{dt} = - \frac{\partial \Pi}{\partial x} + (A_H + \nu) \frac{\partial^2 u}{\partial x^2} + \frac{\partial}{\partial z} \left[(A_V + \nu) \frac{\partial u}{\partial z} \right] ; \qquad (A6a)$$

$$\frac{dw}{dt} = - \frac{\partial \Pi}{\partial z} + g\sigma_t \cdot 10^{-3} + (A_H + \nu) \frac{\partial^2 w}{\partial x^2} + \frac{\partial}{\partial z} \left[(A_V + \nu) \frac{\partial w}{\partial z} \right] \quad ; \qquad (A6b)$$

$$\frac{dT}{dt} = (K_H^T + \kappa) \frac{\partial^2 T}{\partial x^2} + \frac{\partial}{\partial z} \left[(K_V^T + \kappa) \frac{\partial T}{\partial z} \right] \quad ; \qquad (A7a)$$

$$b \frac{dS}{dt} = - \frac{\partial}{\partial x} (buS) - \frac{\partial}{\partial z} (bwS) + \frac{\partial}{\partial x} (bK_H^S \frac{\partial S}{\partial x}) + \frac{\partial}{\partial z} (bK_V^S \frac{\partial S}{\partial z}) ; \qquad (A7b)$$

where $\Pi = p - p_0$ and $\nu = \mu/\rho_0$; $\rho = (1 + \sigma_t \cdot 10^{-3})$.

Transformed non-dimensional model equations, Bork (1978):

Transformation: $\{-\frac{\partial u}{\partial z} + \frac{\partial w}{\partial x} \rightarrow \xi\}$; $\xi \hat{=}$ vorticity

Introduce ψ ə $u = -\frac{1}{b}\frac{\partial \psi}{\partial z}$ and $w = \frac{1}{b}\frac{\partial \psi}{\partial x}$; $\psi \hat{=}$ stream function

$$\frac{d\xi}{dt} = Fr^{-2} \cdot 10^{-3} \frac{\partial \sigma_t}{\partial x} + Pr \cdot \varepsilon \delta_A \left(1 + \frac{\nu}{A_H}\right) \frac{\partial^2 \xi}{\partial x^2} + Pr \cdot \varepsilon \frac{\partial}{\partial z}\left[\left(V_{mix} + \frac{\kappa}{A_V}\right) \frac{\partial \xi}{\partial z}\right] ; \qquad (A8)$$

$$\xi = \frac{1}{b}\left(\frac{\partial^2 \psi}{\partial z^2} + \frac{\partial^2 \psi}{\partial x^2}\right) ; \qquad (A9)$$

$$\frac{\partial X}{\partial t} = \varepsilon \delta_K \left(1 + \frac{\kappa}{K_V X}\right) \frac{\partial^2 X}{\partial x^2} + \varepsilon \frac{\partial}{\partial z}\left[\left(V_{mix} + \frac{\kappa}{K_V X}\right) \frac{\partial X}{\partial z}\right] ; \quad X = T,S ; \qquad (A10a,b)$$

where $\delta_K = K_H/K_V$; $\delta A = A_H/A_V$;

$V_{mix} = K_V(z)/K_V$ scale;

$\varepsilon = K_V\, t_{scale}/L_{scale}$;

$Pr = A_V/K_V$;

$$Fr = \frac{u_{scale}}{\sqrt{gL_{scale}}} .$$

Appendix II

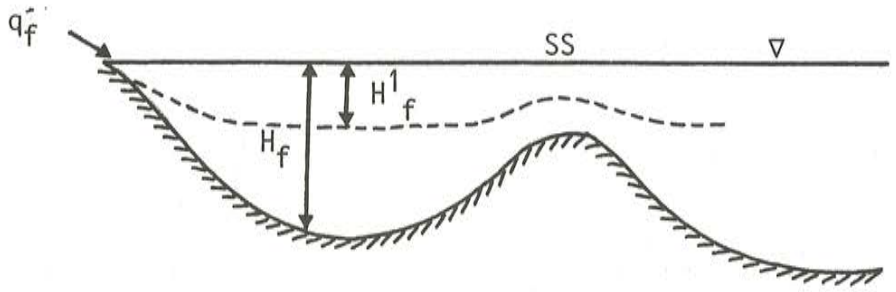

Estuarian flow in a fjord with a narrow rectangular mouth, according to Stigebrandt (1975):

$$P^3\left(1+\frac{\eta^3}{(1-\eta)^3}\right)-2P^2+P=\frac{\eta^3}{F_e^{\,2}}\ ; \qquad (6) = (B1)$$

$$\frac{P^3}{(1-\eta)^3}F_e^{\,2}-(P^3-2P^2+P)\frac{F_e^{\,2}}{\eta^2(1-\eta)}+2=\frac{P^3}{(1-\eta)}F_e^{\,2}R^2H_m^{\,2}\left[\frac{1}{H_{1f}^{\,2}}-\frac{1}{(H_f-H_{1f})^2}\right]+\frac{2H_{1f}}{H_m(1-\eta)} \qquad (B2)$$

$$P=\frac{q'_f\ g\beta S_2 H_{1_f}}{q'_f g\beta H_{1f}-K_h u_*^{\,3}A}\ ; \qquad (B3)$$

$$R=\frac{l_m}{l_f}\quad ;\ u_* = 1.25\cdot10^{-3}W\quad ;\quad K_h = 2.5$$

$$\left.\begin{aligned} q'_f &= 10\ m^3/s \\ \beta &= 8\cdot10^{-4} \\ S_2 &= 6\ ‰ \\ H_m &= 10.5\ m \\ B_m &= 300 = l_m \\ H_f &= 15\ m \\ l_f &= 1000\ m \\ A &= 27\cdot10^6 m^2 \end{aligned}\right\} \Rightarrow W(P,\eta) \text{ according to picture 17.}$$

LIST OF SYMBOLS (not including Appendix I)

A	area
A_H	horizontal eddy viscosity
A_V	vertical eddy viscosity
B_m $(=l_m)$	width of fjord mouth
c_d	drag coefficient
D	depth of basin
F_{di}	estuarine Froude number for layer No. i
F_e	estuarine Froude number
f	Coriolis frequency
g	acceleration of gravity
g'	reduced gravity
H_i	depth of layer i
H_m	depth at fjord mouth
K_H	horizontal eddy viscosity
K_V	vertical eddy viscosity
l_i	width of
l_f	width of fjord
l_m $(=B_m)$	width of fjord mouth
L	Length of estuary
P	estuarine flow/freshwater flow ratio
Qe	estuarine flow
Q_f $(=q'_f)$	freshwater flow
Q_w	wind-driven flow
Q_{wl}	water level change induced flow
r	correlation coefficient
$\bar{r}$	averaged correlation coefficient
Ri	Richardson number
S	salinity
t	time
T	Temperature
T_s	seiche period
u, v, w	velocities in x, y, z directions respectively
W	windspeed
x, y, z	Cartesian coordinate system
β	salinity-to-density conversion factor
Δx, Δz	grid point distances in x and z direction respectively
Δt	time step
η	quotient lower layer/total depth
λ	Rossby radius
ρ	density
ρ_a	density of air
τ_f	time constant to achieve steady-state
τ_w	wind stress
τ_w^*	critical wind stress

REFERENCES

Bergstrand, E. (1977) Strömmätningar i Himmerfjärden 1976. Report No. HB 26, SMHI.

Bergstrand, E. (1980) Utvärdering av området akvatisk ekologi. Report to NFR (Swedish Natural Sci. Res. Council).

Bork, I. (1978) Preliminary model studies of sinking plumes. Report No. RHO 14, SMHI.

Buch, E. (1980) Turbulent mixing and particle distribution investigations in the Himmerfjärd 1978. Report No. RHO 26, SMHI.

Engqvist, A. (1982) Vattenomsättningen i Himmerfjärden 1977 - Ett försök till postdiktion. Report to SNV.

Hamilton, P. & M. Rattray, Jr. (1978) Theoretical aspects of estuarine circulation. In: B. Kjerfve (ed.), Estuarine Transport Processes. Univ. of South Carolina Press, pp. 37-44.

Jörgensen, S. E. (1979) Handbook of environmental data and ecological parameters. ISEM, Copenhagen.

Kullenberg, G. (1971) Vertical diffusion in shallow waters. Tellus XXIII, 2.

Kullenberg, G. (1976) On vertical mixing and the energy transfer from the wind to the water. Tellus XXVIII, 2.

Landau, L. D. & E. M. Lifshitz (1959) Fluid mechanics. Course of Theoretical Physics Vol. 6, Pergamon Press, London.

Rattray, Jr., M. & D. V. Hansen (1962) A similarity solution for circulation in an estuary. J. of Marine Research Vol. 20, No. 2.

Roach, P. J. (1972) Computational fluid dynamics. Hermosa publishers, Albuquerque.

Rydberg, L. (1981) Byfjorden - Tröskelflödets betydelse för vattenomsättning och hydrografi. Vatten, Vol. 2, Lund, pp. 122-143.

Stigebrandt, A. (1975) Stationär tvålagerströmning i estuarier. Report No. STF60 A75120a., VHL, Trondheim.

Stigebrandt, A. (1981) Water exchange between the sea and complicated fjords with special reference to the Baltic water exchange. In: H. Gade, Edwards, A. and Svendsen, H. (eds.), Coastal Oceanography. Plenum Press, pp. 427-437.

Stigebrandt, A. (1982) Element av fjorddynamikken. Report No. STF60 A82096, VHL, Trondheim.

Stigebrandt, A. (1983) A mechanism governing the estuarine circulation in deep, strongly stratified fjords. Estuarine, Coastal and Shelf Sci., Vol. 13, pp. 197-211.

Stommel, H. & Farmer, H. G. (1953) Control of salinity in an estuary by a transition. J. of Marine Research, Vol. XII, 1, pp. 13-20.

Svensson, J. and Wilmot, W. (1978) A numerical model of the circulation in Öresund. Evaluation of the effect of a tunnel between Helsingborg and Helsingör. Report No. RHO 15, SMHI.

Svensson, J. (1980) Sinking cooling water plumes in a numerical model. Report No. RHO 23, SMHI.

Svensson, T. (1980) Water exchange and mixing in fjords. Report No. A7, Dept. of Hydraulics, CTH, Gothenburg.

Toll, P. (1980) Materialtransporter i Himmerfjärden. Report to SNV.

Wilmot, W. (1976) A numerical model of the effect of reactor cooling water on fjord circulation. Report No. RHO 6, SMHI.

SMHI
HO
kuy/L/SCR

SMHI Rapporter, HYDROLOGI OCH OCEANOGRAFI (RHO)

Nr 1 Weil, J G
Verification of heated water jet numerical model
Stockholm 1974

Nr 2 Svensson, J
Calculation of poison concentrations from a hypothetical accident off the Swedish coast
Stockholm 1974

Nr 3 Vasseur, B
Temperaturförhållanden i svenska kustvatten
Stockholm 1975

Nr 4 Svensson, J
Beräkning av effektiv vattentransport genom Sunninge sund
Stockholm 1975

Nr 5 Bergström, S och Jönsson, S
The application of the HBV runoff model to the Filefjell research basin
Norrköping 1976

Nr 6 Wilmot, W
A numerical model of the effects of reactor cooling water on fjord circulation
Norrköping 1976

Nr 7 Bergström, S
Development and application of a conceptual runoff model
Norrköping 1976

Nr 8 Svensson, J
Seminars at SMHI 1976-03-29--04-01 on numerical models of the spreading of cooling water
Norrköping 1976

Nr 9 Simons, J, Funkquist, L and Svensson, J
Application of a numerical model to Lake Vänern
Norrköping 1977

Nr 10 Svensson, S
A statistical study for automatic calibration of a conceptual runoff model
Norrköping 1977

Nr 11 Bork, I
Model studies of dispersion of pollutants in Lake Vänern
Norrköping 1977

Nr 12 Fremling, S
Sjöisars beroende av väder och vind, snö och vatten
Norrköping 1977

Nr 13 Fremling, S
Sjöisars bärighet vid trafik
Norrköping 1977

Nr 14 Bork, I
Preliminary model studies of sinking plumes
Norrköping 1978

Nr 15 Svensson, J and Wilmot, W
A numerical model of the circulation in Öresund
Evaluation of the effect of a tunnel between Helsingborg and Helsingör
Norrköping 1978

Nr 16 Funkquist, L
En inledande studie i Vätterns dynamik
Norrköping 1978

Nr 17 Vasseur, B
Modifying a jet model for cooling water outlets
Norrköping 1979

Nr 18 Udin, I och Mattsson, I
Havsis- och snöinformation ur datorbearbetade satellitdata - en metodstudie
Norrköping 1979

Nr 19 Ambjörn, C och Gidhagen, L
Vatten- och materialtransporter mellan Bottniska viken och Östersjön
Norrköping 1979

Nr 20 Gottschalk, L och Jutman, T
Statistical analysis of snow survey data
Norrköping 1979

Nr 21 Eriksson, B
Sveriges vattenbalans. Årsmedelvärde (1931-60) av nederbörd, avdunstning och avrinning
Norrköping 1980

Nr 22 Gottschalk, L and Krasovskaia, I
Synthesis, processing and display of comprehensive hydrologic information
Norrköping 1980

Nr 23 Svensson, J
Sinking cooling water plumes in a numerical model
Norrköping 1980

Nr 24 Vasseur, B, Funkquist, L and Paul, J F
Verification of a numerical model for thermal plumes
Norrköping 1980

Nr 25 Eggertsson, L-E
HYPOS - ett system för hydrologisk positionsangivelse
Norrköping 1980

Nr 26 Buch, Erik
Turbulent mixing and particle distribution investigations in the Himmerfjärd 1978
Norrköping 1980

Nr 27 Eriksson, B
Den "potentiella" evapotranspirationen i Sverige
Norrköping 1980

Nr 28 Broman, B
On the spatial representativity of our oceanographic measurements
Norrköping 1981

Nr 29 Ambjörn, C, Luide, T, Omstedt, A, Svensson, J
En operationell oljedriftsmodell för norra Östersjön
Norrköping 1981

Nr 30 Svensson, J
Vågdata från svenska kustvatten 1979 - 1980
Norrköping 1981

Nr 31 Jutman, T
Stationsnät för vattenföring
Norrköping 1981

Nr 32 Omstedt, A, Sahlberg, J
Vertical mixing and restratification in the Bay of Bothnia during cooling
Norrköping 1982

Nr 33 Brandt, M
Sedimenttransport i svenska vattendrag
Norrköping 1982

Nr 34 Bringfelt, B
A forest evapotranspiration model using synoptic data
Norrköping 1982

Nr 35 Bhatia, P K, Bergström, S, Persson, M
Application of the distributed HBV-6 model to the Upper Narmada Basin in India
Norrköping 1984

Nr 36 Omstedt, A
A forecasting model for water cooling in the Gulf of Bothnia and Lake Vänern
Norrköping 1984

Nr 37 Gidhagen, L
Coastal Upwelling in the Baltic - a presentation of satellite and in situ measurements of sea surface temperatures indicating coastal upwelling
Norrköping 1984

Nr 38 Engqvist, A, Svensson, J
Water turnover in Himmerfjärd 1977 - a simulation study
Norrköping 1984

SMHI
HO
kuy/L/SCR

SMHI Rapporter, METEOROLOGI OCH KLIMATOLOGI (RMK)

Nr 1 Thompson, T, Udin, I, and Omstedt, A
Sea surface temperatures in waters surrounding Sweden
Stockholm 1974

Nr 2 Bodin, S
Development on an unsteady atmospheric boundary layer model.
Stockholm 1974

Nr 3 Moen, L
A multi-level quasi-geostrophic model for short range weather predictions
Norrköping 1975

Nr 4 Holmström, I
Optimization of atmospheric models
Norrköping 1976

Nr 5 Collins, W G
A parameterization model for calculation of vertical fluxes of momentum due to terrain induced gravity waves
Norrköping 1976

Nr 6 Nyberg, A
On transport of sulphur over the North Atlantic
Norrköping 1976

Nr 7 Lundqvist, J-E, and Udin, I
Ice accretion on ships with special emphasis on Baltic conditions
Norrköping 1977

Nr 8 Eriksson, B
Den dagliga och årliga variationen av temperatur, fuktighet och vindhastighet vid några orter i Sverige
Norrköping 1977

Nr 9 Holmström, I, and Stokes, J
Statistical forecasting of sea level changes in the Baltic
Norrköping 1978

Nr 10 Omstedt, A, and Sahlberg, J
Some results from a joint Swedish-Finnish sea ice experiment, March, 1977
Norrköping 1978

Nr 11 Haag, T
Byggnadsindustrins väderberoende, seminarieuppsats i företagsekonomi, B-nivå
Norrköping 1978

Nr 12 Eriksson, B
Vegetationsperioden i Sverige beräknad från temperaturobservationer
Norrköping 1978

Nr 13 Bodin, S
En numerisk prognosmodell för det atmosfäriska gränsskiktet grundad på den turbulenta energiekvationen
Norrköping 1979

Nr 14 Eriksson, B
Temperaturfluktuationer under senaste 100 åren
Norrköping 1979

Nr 15 Udin, I, och Mattisson, I
Havsis- och snöinformation ur datorbearbetade satellitdata - en modellstudie
Norrköping 1979

Nr 16 Eriksson, B
Statistisk analys av nederbördsdata. Del I. Arealnederbörd
Norrköping 1979

Nr 17 Eriksson, B
Statistisk analys av nederbördsdata. Del II. Frekvensanalys av månadsnederbörd
Norrköping 1980

Nr 18 Eriksson, B
Årsmedelvärden (1931-60) av nederbörd, avdunstning och avrinning
Norrköping 1980

Nr 19 Omstedt, A
A sensitivity analysis of steady, free floating ice
Norrköping 1980

Nr 20 Persson, C och Omstedt, G
En modell för beräkning av luftföroreningars spridning och deposition på mesoskala
Norrköping 1980

Nr 21 Jansson, D
Studier av temperaturinversioner och vertikal vindskjuvning vid Sundsvall-Härnösands flygplats
Norrköping 1980

Nr 22 Sahlberg, J and Törnevik, H
A study of large scale cooling in the Bay of Bothnia
Norrköping 1980

Nr 23 Ericson, K and Hårsmar, P-O
Boundary layer measurements at Klockrike. Oct. 1977
Norrköping 1980

Nr 24 Bringfelt, B
A comparison of forest evapotranspiration determined by some independent methods
Norrköping 1980

Nr 25 Bodin, S and Fredriksson, U
Uncertainty in wind forecasting for wind power networks
Norrköping 1980

Nr 26 Eriksson, B
Graddagsstatistik för Sverige
Norrköping 1980

Nr 27 Eriksson, B
Statistisk analys av nederbördsdata. Del III. 200-åriga nederbördsserier
Norrköping 1981

Nr 28 Eriksson, B
Den "potentiella" evapotranspirationen i Sverige
Norrköping 1981

Nr 29 Pershagen, H
Maximisnödjup i Sverige (perioden 1905-70)
Norrköping 1981

Nr 30 Lönnqvist, O
Nederbördsstatistik med praktiska tillämpningar
(Precipitation statistics with practical applications)
Norrköping 1981

Nr 31 Melgarejo, J W
Similarity theory and resistance laws for the atmospheric boundary layer
Norrköping 1981

Nr 32 Liljas, E
Analys av moln och nederbörd genom automatisk klassning av AVHRR data
Norrköping 1981

Nr 33 Ericson, K
Atmospheric Boundary layer Field Experiment in Sweden 1980, GOTEX II, part I
Norrköping 1982

Nr 34 Schoeffler, P
Dissipation, dispersion and stability of numerical schemes for advection and diffusion
Norrköping 1982

Nr 35 Undén, P
The Swedish Limited Area Model (LAM). Part A. Formulation
Norrköping 1982

Nr 36 Bringfelt, B
A forest evapotranspiration model using synoptic data
Norrköping 1982

Nr 37 Omstedt, G
Spridning av luftförorening från skorsten i konvektiva gränsskikt
Norrköping 1982

Nr 38 Törnevik, H
An aerobiological model for operational forecasts of pllen concentration in th air
Norrköping 1982

Nr 39 Eriksson, B
Data rörande Sveriges temperaturklimat
Norrköping 1982

Nr 40 Omstedt, G
An operational air pollution model using routine meteorological data
Norrköping 1984

Nr 41 Christer Persson and Lennart Funkquist
Local scale plume model for nitrogen oxides.
Model description.

Nr 42 Stefan Gollvik
Estimation of orographic precipitation by dynamical interpretation of synoptic model data.

ISSN 0347-7827

SMHI

SWEDISH METEOROLOGICAL AND HYDROLOGICAL INSTITUTE
S-60176 Norrköping, Sweden. Tel. +46 11 15 80 00. Telex 64400 smhi s.